Toxicon 234 (2023) 107285

Contents lists available at ScienceDirect

Toxicon

journal homepage: www.elsevier.com/locate/toxicon

Comparing morphological and secretory aspects of cephalic glands among the New World coral snakes brings novel insights on their biological roles

Leonardo de Oliveira [a,b,1,*], Pedro Gabriel Nachtigall [a,1], Vincent Louis Vialla [a], Pollyanna F. Campos [a], Adriana da Costa-Neves [c], Hussam Zaher [d], Nelson Jorge da Silva Jr. [e], Felipe G. Grazziotin [f], Mark Wilkinson [b], Inácio L.M. Junqueira-de-Azevedo [a]

[a] Laboratório de Toxinologia Aplicada, Centre of Toxins, Immune-Response and Cell Signaling (CeTICS), Instituto Butantan, São Paulo, 05503-900, Brazil
[b] Herpetology, The Natural History Museum, London, SW7 5BD, United Kingdom
[c] Laboratório de Genética, Instituto Butantan, São Paulo, 05503-900, Brazil
[d] Museu de Zoologia da Universidade de São Paulo, Avenida Nazaré 481, Ipiranga, 04263-000, São Paulo, Brazil
[e] Programa de Pós-Graduação em Ciências Ambientais e Saúde, Pontifícia Universidade Católica de Goiás, Goiânia, Goiás, 74605-140, Brazil
[f] Laboratório de Coleções Zoológicas, Instituto Butantan, São Paulo, 05503-900, Brazil

ARTICLE INFO

Handling editor: Ray Norton

Keywords:
Venom glands
Infralabial glands
Rictal glands
Harderian glands
Front-fanged snakes
Micro-CT scan

ABSTRACT

Oral and other cephalic glands have been surveyed by several studies with distinct purposes. Despite the wide diversity and medical relevance of the New World coral snakes, studies focusing on understanding the biological roles of the glands within this group are still scarce. Specifically, the venom glands of some coral snakes were previously investigated but all other cephalic glands remain uncharacterized. In this sense, performing morphological and molecular analysis of these glands may help better understand their biological role. Here, we studied the morphology of the venom, infralabial, rictal, and harderian glands of thirteen species of *Micrurus* and *Micruroides euryxanthus*. We also performed a molecular characterization of these glands from selected species of *Micrurus* using transcriptomic and proteomic approaches. We described substantial morphological variation in the cephalic glands of New World coral snakes and structural evidence for protein-secreting cells in the inferior rictal glands. Our molecular analysis revealed that the venom glands, as expected, are majorly devoted to toxin production, however, the infralabial and inferior rictal glands also expressed some toxin genes at low to medium levels, despite the marked morphological differences. On the other hand, the harderian glands were dominated by the expression of lipocalins, but do not produce toxins. Our integrative analysis, including the prediction of biological processes and pathways, helped decipher some important traits of cephalic glands and better understand their biology.

1. Introduction

Elapids constitute a successful radiation of venomous snakes within Caenophidia with more than 380 species distributed throughout the American, African, Asian, and Australian continents, and in the tropical waters of the Indian and Pacific oceans (Campbell and Lamar, 1989, 2004; Uetz et al., 2021). The Elapidae includes well known iconic taxa such as cobras, kraits, and coral snakes, the latter encompassing the Nearctic and Neotropical representatives of the family (Campbell and Lamar, 1989, 2004; Zaher et al., 2019, 2021). Despite its medical importance (WHO, 2010), little is known about the morphological variation of cephalic glands and the composition of the secretions produced by these glands. Most published data on cephalic gland morphology are focuses on the venom gland (VG) (Rosenberg, 1967; Gopalakrishnakone and Kochva, 1990; Dashevsky et al., 2021) of marine and terrestrial species from Africa and Australia (Old World species), with relatively little attention applied to coral snakes, particularly to the New World species.

Although studies evaluating the composition of venoms produced by elapid VGs are more abundant than those evaluating VG morphology,

* Corresponding author. Laboratório de Toxinologia Aplicada, Center of Toxins, Immune-Response and Cell Signaling (CeTICS), Instituto Butantan, São Paulo, 05503-900, Brazil.
E-mail addresses: leooliveira.herpeto@gmail.com, l.oliveira29@unesp.br (L. Oliveira).
[1] These authors contributed equally to this work.

https://doi.org/10.1016/j.toxicon.2023.107285
Received 6 June 2023; Received in revised form 5 September 2023; Accepted 6 September 2023
Available online 7 September 2023

they are generally focused on lineages with medical importance (i.e., higher incidence of human accidents). Therefore, most of these studies are also concentrated on African and Australasian elapids, and few integrative venomic studies have been developed addressing the diversity of American coral snakes (Aird et al., 2017; Dashevsky and Fry, 2018).

New World coral snakes are a monophyletic group of more than 80 species allocated in the genera *Micrurus* Wagler, 1824, *Leptomicrurus* Schmidt, 1937 (currently a junior synonymy of *Micrurus*; non-consensual), and *Micruroides* Schmidt, 1928 (Slowinski, 1995; Roze, 1996; Silva Jr et al., 2021a; Zaher et al., 2019, 2021; Uetz et al., 2021). The genus *Micrurus* is by far the most diverse within the group. *Leptomicrurus* is composed of only three species, and *Micruroides* is a monospecific genus (Slowinski, 1995; Roze, 1996; Silva Jr et al., 2021a; Zaher et al., 2019, 2021; Uetz et al., 2021).

The VGs of New World coral snakes present the general morphological pattern of a typical elapid VG, which has been described by numerous authors (e.g., Rosenberg, 1967; Burns and Pickwell, 1972; Gopalakrishnakone and Kochva, 1990). They are frequently ovoid or pear-shaped in lateral view and occupy practically the entire postocular region. Elapid VGs are composed of two portions (Kochva, 1978), a VG proper, and an accessory gland (AG). A duct that drains the VG passes through the AG and opens into the sheath of the fang (Oliveira et al., 2021). The central lumen is relatively small, and, differently from viperids, the secretion is stored mainly in intracellular secretion granules (Kochva, 1987). Elapid VGs are compressed by the fibres derived from the *adductor mandibularis externus superficialis* muscle, which in most elapids has a dorsal and a ventral portion (McDowell, 1968; McCarthy, 1985; Zaher, 1994). Although the general pattern of elapid VGs and compressing musculature is relatively conserved in all elapids studied, the atractaspidid *Homoroselaps* exhibit similar structures, indicating an independent derivation of this glandular and muscular morphology (McDowell, 1968; McCarthy, 1985; Oliveira and Zaher, 2022). In addition, while presenting an extensive morphological variation and distinctive pattern between different families, the VGs of snakes are a type of dental gland that appear to be homologous and restricted to the clade Endoglyptodonta, a lineage of caenophidian snakes composed of front-fanged and non-front-fanged species, including viperids, homalopsids, elapoids, and colubroids (Kochva, 1978, 1987; Underwood and Kochva, 1993; Zaher et al., 2019; Oliveira and Zaher, 2022).

Transcriptomic and proteomic analyses of VGs have showed that two toxin classes—phospholipases A2 (PLA_2) and three-finger α-neurotoxins (3FTx)—dominate the venom composition of New World coral snakes (Aird et al., 2017; Sanz et al., 2016). These toxins can result in muscle paralysis and respiratory arrest (Corrêa-Netto et al., 2011; Bucaretchi et al., 2021), and they can present presynaptic (PLA_2) or postsynaptic (3FTx) effects. Additionally, VGs of *Micrurus* can express significant levels of other toxins like C-type natriuretic peptide, Kunitz-type protease inhibitor, and snake venom metalloproteinases (Margres et al., 2013; Aird et al., 2017; Dashevsky and Fry, 2018).

On the other hand, the glands in the inferior part of the jaw are much less studied. In a recent morphological evaluation, Oliveira et al. (2021) showed that *Micrurus corallinus* and *Micrurus lemniscatus* have an inferior gland complex, consisting of distinct anterolateral and posteromedial parts. The anterolateral part consists predominantly of mucous cells and possesses diverse short ducts opening along the entire extension of the mouth, indicating that it is a typical infralabial gland (ILG) (Underwood, 2002; Jackson et al., 2017; Oliveira and Zaher, 2022). The posteromedial part consists exclusively of serous cells and possesses a single duct opening in the posterior region of the mouth, indicating that this is a rictal gland (RG) (Underwood, 1997; Oliveira et al., 2021). Despite this recent contribution, the morphology of ILGs and RGs of most species in the highly diverse group of New World coral snakes remains unknown.

Concerning the functional activity of the secretions produced by the glands of the inferior portion of the jaw of micrurines, a study on *M. mosquitensis* suggested that secretions from the ILG have toxic effects when injected intraperitoneally in mice, causing similar symptoms to those observed in cases of coral snakes' envenomation (Dix, 1978). However, the secretion of these glands has never been evaluated so far through proteomic or transcriptomic methods, and thus, their composition is almost completely unknown.

RGs are the most enigmatic cephalic glands in snakes. They are reported in several species, including caenophidian and non-caenophidian snakes (e.g., Phisalix, 1922; Smith and Bellairs, 1947; Gabe and Saint-Girons, 1969; McDowell, 1986; Underwood, 1997, 2002; Oliveira and Zaher, 2022) and have been attributed with various putative functions such as venom production, lubrication, and antimicrobial defence (Jackson et al., 2017). These glands are associated with the corner of the mouth, but little is known about their homology. In different snakes, RGs can be either completely absent or present in association with the maxilla (superior RG), the mandible (inferior RG), or both (superior and inferior RG) (McDowell, 1986; Underwood, 1997, 2002; Zaher, 1997; Wollberg et al., 1998; Oliveira and Zaher, 2022). Among elapids, these glands were reported so far to occur in only a few species, with superior RGs being more often documented than inferior RGs (Underwood, 1997; Wollberg et al., 1998; Jackson et al., 2017). Unlike the RGs, the ILGs seem to occur in all snakes and lizards that have been studied (Kochva, 1978; Underwood, 2002; Jackson et al., 2017; Oliveira and Zaher, 2022). The limited knowledge of the morphological diversity and taxonomic distribution of RGs in elapids has prevented the formation of any hypotheses regarding the function of these glands. Moreover, the complete lack of knowledge regarding the composition of secretions produced by RGs and ILGs makes it challenging to interpret the preliminary findings that suggest the toxic effect of the ILG secretions from *Micrurus* (Dix, 1978).

Another poorly studied cephalic gland in snakes is the Harderian gland (HG). This gland is present in most tetrapods, including all families of snakes (Taub, 1966; Parson, 1970; Hillenius and Rehorek, 2005), and functions in the lubrication of the eye and as an auxiliary organ involved in vomeronasal chemosensation (Saint-Girons, 1982; Rehorek et al., 2000a; Hillenius and Rehorek, 2005). In most snakes where this gland has been investigated it is serous and located behind the eyes. Although the HG is not usually considered an oral gland, it is indirectly connected to the mouth in snakes (Bellairs and Boyd, 1947; Taub, 1966). Until now, there is no comparative evaluation of the morphology of this gland among *Micrurus*. Moreover, the secretion composition of HG was not characterized in this genus yet.

To advance the knowledge about cephalic glands (VGs, RGs, ILGs, and HGs) in New World elapids, we thoroughly evaluate their morphological structure and molecular composition. We provide a detailed morphological characterization of these glands for *Micruroides euryxanthus* and for 14 species of *Micrurus*. Additionally, we describe and compare profiles of gene expression (transcriptomes) and protein composition (proteomes) for cephalic glands of four species of *Micrurus*. Comparative analysis of morphological and molecular data allowed us to predict functional specialization in cephalic glands, shedding light on the biological roles of the cephalic secretory system in snakes.

2. Material and methods

2.1. Species studied and general morphology

Fourteen New World micrurine species were investigated. The complete list of taxa examined, and the procedures performed with each specimen are in Table 1 in Supplementary file 1. For specimens used in the study of general morphology, heads were skinned from the nostril to the neck and removed from the specimens at the level of the first cervical vertebra. Then, the skinned heads were stained with alcian blue and alizarin red and used for anatomical description of glands and muscles. The dissections were performed under a stereomicroscope Olympus SZX 12 equipped with a camera lucida. Glandular terminology follows Taub (1966), Kochva (1978), and Underwood (2002). The terminology of the

Table 1
List of the fifteen most expressed orthogroups of each studied gland. The expression values represents TPM (transcripts per milion reads).

Order	Gland type	Orthogroup	Average (TPM)	Mcor (TPM)	Mtri (TPM)	Mlem (TPM)	Malt (TPM)	General description of best NCBI hits (Blast X)
1°	Venom	OG0000185_3FTx	203245.20	340033.72*	3038.92*	178707.9*	291200.25	Three-finger toxin
2°	Venom	OG0000056_3FTx	75659.53	126030.64*	23348.86*	142306.49*	10952.12	Three-finger toxin
3°	Venom	OG0000023_PLA2	69776.96	64159.54*	125587.61*	68223.34*	21137.35	Phospholipase A2
4°	Venom	OG0000186_KUNZ	35814.93	1050.01	67682.43*	62229.27*	12298.03	Kunitz inhibitor precursor
6°	Venom	OG0001644_3FTx	21915.25	81485.68*	964.45*	1758.28*	3452.58	Three-finger toxin
7°	Venom	OG0000810	9128.31	10654.49*	11575.24*	5867.21*	8416.30	Protein disulfide-isomerase
8°	Venom	OG0000248	7416.53	6142.77	6146.88	8530.93	8845.56	No significant similarity found
9°	Venom	OG0000592_CTL	3789.24	9361.36*	3258.67*	678.76*	1858.16	C-type lectin
10°	Venom	OG0000022	3142.42	1574.68*	1442.56*	6677.07*	2875.37	Actin
11°	Venom	OG0002231	2636.96	2109.18	2884.52	3456.59	2097.55	60S ribosomal protein
12°	Venom	OG0000108	2600.82	2401.99*	2251.58*	2909.33*	2840.39	Elongation factor 1-alpha 2
14°	Venom	OG0000962	2284.21	2159.76	1913.94	2176.15	2887.0	40S ribosomal protein
15°	Venom	OG0001719	2094.98	1822.75	1650.31	2409.22*	2497.63	60S ribosomal protein
14°	Venom	OG0001743	2025.86	2545.95	1983.75	880.41	2693.32	Translocation chain-associated membrane
15°	Venom	OG0003140	1991.63	2381.72	2386.11	3000.5	198.2	40S ribosomal protein S29
1°	Rictal	OG0000956_CTL	34174.49	19486.05*	11412.8*	71624.62*	–	C-type lectin precursor
2°	Rictal	OG0000090	29687.50	31582.52*	43826.86*	13653.13*	–	Chitotriosidase-1
3°	Rictal	OG0000053	22851.23	12.67	3765.97*	64775.04*	–	Hypothetical protein
4°	Rictal	OG0000012	19423.29	3246.49	632.13	54391.26*	–	Ficolin
5°	Rictal	OG0000014	16984.07	9615.74*	40239.20*	1097.26*	–	Immunoglobulin
6°	Rictal	OG0000248	9639.21	9841.44	11739.36	7336.83	–	No significant similarity found
7°	Rictal	OG0000104	7807.68	371.89	712.45	22338.7	–	Ficolin
8°	Rictal	OG0000164	6689.27	7781.02*	1438.05*	10848.74*	–	Serotransferin
9°	Rictal	OG0000253_CTL	6151.07	11787.09*	3931.28*	2734.85	–	C-type lectin
10°	Rictal	OG0000593_CRISP	5543.19	8003.77*	381.79*	8243.99*	–	Cystein-rich secretory protein
11°	Rictal	OG0000372_CTL	5279.88	4551.85	6030.20*	5257.6	–	C-type lectin
12°	Rictal	OG0000185_3FTx	4555.10	7.60	13635.88*	21.8	–	Three-finger toxin
13°	Rictal	OG0000206	4098.24	3067.41*	3957.43*	5269.90*	–	Alpha-2-macroglobulin
14°	Rictal	OG0000367_CTL	3837.04	9431.53*	1956.43	123.18	–	C-type lectin
15°	Rictal	OG0002231	3684.25	5139.71	3447.07*	2465.96*	–	60S ribosomal protein
1°	Infralabial	OG0000014	23382.31	9385.76*	57102.97*	6773.02*	20267.46	Immunoglobulin
2°	Infralabial	OG0000956_CTL	22967.67	11827.45*	21055.18*	48778.07*	10209.98	C-type lectin
3°	Infralabial	OG0000253_CTL	22070.34	49318.83*	27005.99*	6523.09	5433.44	C-type lectin
4°	Infralabial	OG0000367_CTL	17578.80	40729.46*	17277.05*	300.5	12008.17	C-type lectin
5°	Infralabial	OG0000090	16495.70	11719.30*	34240.18*	7602.58	12420.72	Chitotriosidase
6°	Infralabial	OG0000012	16299.12	2546.72	394.37	61335.15*	920.25	Ficolin
7°	Infralabial	OG0000164	14309.25	19132.18*	13134.94*	12584.81*	12385.04	Serotranferin
8°	Infralabial	OG0000104	9525.19	289.34	479.02	37251.42	80.96	Ficolin
9°	Infralabial	OG0000679	9080.56	19380.38*	2970.71*	7849.01*	6122.12	von Willebrand factor A
10°	Infralabial	OG0000248	8988.40	6685.44	13397.36	6982.22	8888.56	No significant similarity found
11°	Infralabial	OG0000372_CTL	7996.39	15811.77*	4607.88*	9640.69*	1925.21	C-type lectin
12°	Infralabial	OG0000593_CRISP	7525.46	22243.97*	1567.12*	5617.33*	673.43	Cystein-rich secretory protein
13°	Infralabial	OG0000081	6989.68	68.6*	50.03	0.045	27840.04	Creatine kinase M type
14°	Infralabial	OG0000732	5340.11	15023.01*	893.24*	3631.96*	1812.24	Uncharacterized protein
15°	Infralabial	OG0000206	5274.25	7189.18*	7105.23*	4910.88*	1891.69	Alpha-2-Macroglobulin-like
1°	Harderian	OG0000102	141943.04	260321.75*	192796.17*	302.76*	114351.46	Lipocalin
2°	Harderian	OG0000179	107015.19	97451.45*	137390.96*	147103.39*	46114.95	Sperm protamine
3°	Harderian	OG0000856	91535.95	95830.23	142494.52	72916.76	54902.27	No significant similarity found
4°	Harderian	OG0003005	29478.91	54646.53*	28728.28*	14634.62*	19906.22	Lipocalin/fatty-acid binding protein
5°	Harderian	OG0002297	15653.78	15429.22*	23353.87*	11316.54*	12515.48	Lipocalin/fatty-acid binding protein
6°	Harderian	OG0001373	15401.67	14127.22*	24844.68*	12666.9*	9967.89	Uncharacterized protein
7°	Harderian	OG0000858	11285.48	12942.34*	16786.30*	11348.71*	4064.55	Glycine-rich cell wall structural protein
8°	Harderian	OG0004584	9885.76	9562.67*	15458.38*	7096.27*	7425.73	Uncharacterized protein LOC113423838
9°	Harderian	OG0000282	9633.56	18.71	19804.23*	10271.4*	8439.91	Hypothetical protein E2320_000605
10°	Harderian	OG0000857	8167.41	9108.93*	10084.55*	7639.68*	5836.46	BPI fold-containing family B member 6-like
11°	Harderian	OG0001890	6845.59	4846.27*	8944.23*	2986.69*	10605.17	Hypothetical protein E2329_013739
12°	Harderian	OG0003004	6326.44	2967.84*	6198.70*	14568.69*	1570.51	Histone acetyltransferase
13°	Harderian	OG0000878	4705.00	968.29	6617.70	9210.62	2023.4	Extensin, partial
14°	Harderian	OG0004747	3294.89	1974.33*	3702.09*	4503.85*	2999.30	C-reactive protein-like
15°	Harderian	OG0004745	3185.62	3276.0*	2618.41*	5065.7*	1782.35	C-reactive protein-like

Asterisks (*) indicate the orthogroups whose transcripts were detected within the glandular proteome via LC-MS/MS. We considered present in proteomes all orthogroups that showed at least one transcript with an exclusive unique spectra count (EUSC).

external mandibular adductor muscles follows that of Zaher (1994).

2.2. Histology and immunohistochemistry

Histological sections were produced from specimens available from scientific collections, according to Table 1 in Supplementary file 1, and the specimens were returned to their collections after processing. After the study of general morphology, some glands and muscles were dissected from the heads and subjected to histological procedures. A single head of *Micrurus corallinus* was submitted to decalcification in 4.13% aqueous EDTA (pH 7.2) for 60 days with the renewal of solution every three days. The decalcified head and the dissected glands and muscles were then dehydrated in ethanol, embedded in paraffin, and submitted to serial sagittal or transverse sectioning. Sections (7 μm) were cut with a Microm HM 340 E microtome with disposable steel blades. Some sections were stained with haematoxylin-eosin (HE) to identify the general structure of the tissues, and some others subjected to immunohistochemistry using the anti-*Micrurus* antivenom produced by

the Instituto Butantan and an anti-horse IgG (Sigma) (whole molecule) conjugated with alkaline phosphatase produced in rabbits used as the secondary antibody. The Fast Red substrate kit (Abcam) was used as a chromogen for the immunohistochemical staining and the nuclear staining was performed with Mayer's haematoxylin. Images of sections were taken with a DFC425 digital camera coupled with a Leica M205a stereoscopic microscope and a Leica M2500 microscope using Leica Application Suite software (v3.8).

2.3. Micro-computed tomography (micro-CT scan)

The soft tissue anatomy of selected micrurine species (see Table 1 in the Supplementary file 1) was also examined using high-resolution Xray computed tomography (micro-CT scan). Entire heads were stained with a solution of 1% iodine–ethanol solution for one week to increase the tissue contrast following Metscher (2009). Heads mounted in Falcon tubes to keep them immobile attached to bags or other containers of alcohol to prevent desiccation during scanning. The scanning procedures were performed using Phoenix v|tome|x m (General Electric Company) located at the Microtomography Laboratory of the Museum of Zoology of the University of São Paulo (MZUSP, Brazil) and the X-Tek Leading X-Ray Technology HMXST 225 located at the Natural History Museum, London, UK (NHM, UK). To acquire high-quality scans in the MZUSP equipment, a microfocus tube 300 was used and different settings were applied. The images acquired in the MZUSP equipment were reconstructed using Datos Reconstruction software (GE Company), whereas the images acquired in the NHM, UK equipment were reconstructed using Ct Pro 3D. The rendering and analysis of the datasets were conducted using the software VG Studio Max (v2.2.3.69611, 64bits). The soft tissues and bones were visualized by adjusting the histogram/threshold density settings of the grayscale.

2.4. Venom milking and oral glands sampling

Thirteen individuals belonging to the four species of *Micrurus* (*M. altirostris*, *M. corallinus*, *M. lemniscatus*, and *M. tricolor*) were used in these procedures (see Table 1 in Supplementary file 1). The venom was extracted from sedated individuals as described previously (Mackessy and Baxter, 2006). Four days after the venom extraction, the animals were euthanised through the administration of a lethal dose of sodium pentobarbital and all oral glands were surgically dissected under a stereoscopic microscope. The animals were handled, and the protocols applied were approved and certified by the ethical committee of the Instituto Butantan (CEUA No. 4479020217). The right glands were preserved in RNAlater (Qiagen) and stored at −80° until RNA extraction, whereas the left glands were preserved in liquid nitrogen and stored at −80° until protein extraction.

2.5. RNA extraction

The total RNA was extracted using the organic extraction method with TRIZOL reagent (Thermo Fisher Scientific), following manufacturer's protocol. The extracted RNA was solubilized in RNase-free water (Sigma Aldrich) and quantified by measuring UV-absorbance at 260 nm using a NanoDrop 1000 (Thermo Fisher Scientific). The RNA quality was assessed using an Agilent 2100 Bioanalyzer system (Agilent Technologies) according to the manufacturer's instructions.

2.6. RNA-seq and pre-processing of reads

The messenger RNA (mRNA) of each sample was purified using the Dynabeads® mRNA DIRECT kit (Ambion) and used to prepare independent cDNA libraries following the protocol for TruSeq™ RNA Sample Preparation Kits v2 (Illumina). The libraries were sequenced using the HiSeq1500 platform (Illumina) and the sequencing layout generated strand-specific paired-end reads (2x150bp). The Illumina adapters and low-quality reads were trimmed using Trim Galore (v0.4.4; https://github.com/FelixKrueger/TrimGalore)! by setting the parameters to remove reads with *phred* scores less than five and a length less than 75 bp. The paired-end reads were merged using PEAR (Zhang et al., 2014) and used to perform transcriptome assembly and quantification.

2.7. Transcriptome assembly, annotation, and quantification

The *de novo* assembly step was designed to retrieve the complete set of toxin transcripts, which relies on the use of several tools and parameters (Holding et al., 2018). Specifically, we used Trinity (v2.8.5; kmer parameter set to 31; Haas et al., 2013), Extender (v1.0; overlap parameters set to 120 and 150; Rokyta et al., 2012), NGen (v14; using the default parameters; Lasergene DNAStar software package; https://www.dnastar.com/t-nextgen-seqman-ngen.aspx), Bridger (r2014-12-01; kmer parameter set to 30; Chang et al., 2015), and rnaSPAdes (v3.13.0; kmer parameters set to 31, 75, and 127; Bushmanova et al., 2019). Then, we combined and clustered with 100% identity all transcripts assembled using the "RemoveRedundancy.py" script available in the ToxCodAn's GitHub repository (https://github.com/pedronachtigall/ToxCodAn/tree/master/scripts). Of note, we considered most of the parameters within each assembler as defined by their defaults, except for the overlap size in Extender and kmer size in Trinity, Bridger, and rnaSPAdes, as described above.

We annotated the toxins using ToxCodAn (v1.0; Nachtigall et al., 2021a) by combining the set of toxins ("*Toxins_RedundancyFiltered*") and putative toxins ("*SPfiltered*"). Then, we performed a manual curation to eliminate false-positive toxin sequences following the guide to VG transcriptomics (Nachtigall et al., 2021a; https://github.com/pedronachtigall/ToxCodAn/tree/master/Guide). We removed chimeric transcripts using the custom *ChimeraKiller* script (https://github.com/masonaj157/ChimeraKiller). To group allelic variations at a single locus and reduce redundancy, we clustered a curated set of toxin CDSs with 99% similarity using cd-hit (Fu et al., 2012).

We used the set of nontoxin transcripts output by ToxCodAn to perform nontoxin annotation. First, we performed CDS prediction using CodAn (v1.0; Nachtigall et al., 2021b) with the full model designed for vertebrates. The predicted CDSs were annotated using the "NonToxinAnnotation.py" script available with the ToxCodAn tool. We set two protein databases: (1) a specific protein database from ToxCodAn (proteinDB; https://github.com/pedronachtigall/ToxCodAn/), which contains peptide sequences annotated in the genomes of two lizard and one snake species available at the Ensembl, and peptide sequences annotated in the venom-gland transcriptome of seven snake species available at the TSA (see Nachtigall et al., 2021a for further details about the protein database); and (2) the Swissprot database (ftp://ftp.ncbi.nlm.nih.gov/blast/db/swissprot.tar.gz). We also set to use the vertebrate HMM models from BUSCO (Waterhouse et al., 2018) to complement the annotation. Please refer to the guide to venom gland transcriptomics for further details about the pipeline and parameters considered by the "NonToxinAnnotation.py" script (Nachtigall et al., 2021a).

Finally, the annotated set of nontoxins was combined with the set of annotated toxins for all tissues studied and clustered with 99% similarity using cd-hit for each gland of each specimen. We combined the individual's annotated transcriptomes of all glands of each species and clustered with 98% similarity to generate a species consensus transcriptome. To perform transcript quantification, we mapped the merged reads to the species consensus transcriptome using Bowtie2 (v2.3.5; Langmead and Salzberg, 2012) and estimated the expression level using RSEM (v1.3.1; Li and Dewey, 2011).

We also performed a phylogenetic inference for the CTL toxin group to better understand their evolutionary history and expression profile in the oral glands. We aligned the coding sequences using MAFFT (v7.450; Rozewicki et al., 2019) with parameters "–auto–reorder", and used IQTree (v1.6.12; Nguyen et al., 2015) with parameters "-m TEST -bb

1000 -alrt 1000" to search for the maximum likelihood tree. The final tree was adjusted using FigTree (v1.4.4; https://github.com/rambaut/figtree/).

2.8. Comparative analysis

To compare the transcriptomic data of cephalic glands, we first inferred orthology among the annotated transcripts (i.e., toxins and nontoxins) of the four *Micrurus* species using OrthoFinder (v2.3.14; Emms and Kelly, 2019). OrthoFinder identifies groups of sequences derived from a common ancestor (i.e., orthogroups), which allows the identification of orthology relationships and further comparative analysis. We only kept orthogroups with one-to-one and all-to-one relationships to perform further analysis. Then, we compared the expression pattern of each gland among species by using the expected count normalized by the DEseq2 package (v1.34; Love et al., 2014) followed by a principal component analysis (PCA) in the normalized expression data using the *plotPCA* function in the *DESeq2 package*.

To predict the biological roles of each gland, we used the set of highly expressed genes in each gland when compared to the other glands, to detect if genes of a particular functional category are enriched based on the gene ontology (GO) approach (Ashburner et al., 2000). The candidate set of highly expressed genes in each gland were captured by performing a pairwise comparison with the other glands using the DEseq2 package. Then, we concatenated all genes up-regulated (i.e., genes with a positive fold-change value and adjusted p-value <0.05) in each pairwise comparison into the candidate set of genes to infer the biological processes specific to each gland. We performed the GO terms enrichment analysis using ShinyGO (v0.75; Ge et al., 2019) with the *Gallus gallus* genome as a reference, a false discovery rate (FDR) cutoff of 0.05 and retrieved the 30 most significant terms. We used the chicken genome as the reference because it represents a closely related database with higher completeness. Other reptilian databases, such as *Anolis carolinensis*, are less complete and do not present functional information matching the set of genes used in each search. We applied the *igraph* package (v1.2.11; Csárdi and Nepusz, 2006) in the R environment to plot networks and cluster dense connections with the algorithm "*cluster_edge_betweenness*."

2.9. Proteomic analysis

We used protein extracted from the glands to perform shotgun liquid chromatography–tandem mass spectrometry analysis. The venom samples were prepared by denaturation with urea, reduction with triethylphosphine, and alkylation with iodoethanol before treatment with trypsin solution (0.2 μg/μL). The protein extracted from gland tissues were performed using a lysis buffer (HEPES 100 mM, CHAPS 2%, and NaCl 200 mM; pH 7,5) with a mix of Halt Protease, Phosphatase Inhibitor Cocktail, and EDTA (Thermo Fisher Scientific). The tissues within the lysis buffer were homogenized using Precellys24 (Thermo Fisher Scientific) in one cycle of 6800 rpm over 60s, followed by sonication with five cycles of 30s. The proteins were precipitated using cold acetone at −20 °C overnight. Then, the proteins were centrifuged (10000g; 1h; 4 °C), washed with cold methanol, and re-centrifuged (10000g; 20min; 4 °C). The proteins were resuspended in a solution containing NaOH (0.1M), phosphatase inhibitor, and protease inhibitor. The solubilized proteins were centrifuged to recover the supernatant and addition of a guanidine (2M) solution followed by addition of HEPES (0.2M) solution. The peptide concentration of each sample was quantified with the Qubit 2.0 Fluorometer (Life Technologies). The shotgun liquid chromatography–tandem mass spectrometry was performed at the University of São Paulo BIOMASS–Core Facility for Scientific Research-USP (CEFAP-USP) by following its guidelines.

The raw data were processed and studied using two computational tools: Mascot (Matrix Science) and Scaffold (v4.9.0; Proteome Software Inc). The database used to identify the spectra is composed of the coding sequences of the consensus transcriptome obtained for each species in the transcriptome assembly step translated into peptide sequences. The Mascot was used to match the peptides into the identified proteins and the Scaffold was used to validate the identification performed by Mascot. Peptide identifications were accepted if they could be established at >99.0% probability at the Scaffold local false discovery rate through the FDR algorithm. Peptide identifications were also required to exceed specific database search engine thresholds, such as Mascot ion scores >40.0 and/or X! Tandem –Log (E-value) score >2.0. Protein identifications were accepted if they could be established at >99.0% probability of achieving an FDR <1.0%. The quantification of proteins related to the general abundance in each gland was based on normalized Total Spectral Counts, which correspond to the number of spectra attributed to proteotypic peptides of a given protein entry present in the database.

3. Results and discussion

3.1. Venom glands

3.1.1. Morphology

The VG is well-developed in all studied species, generally oval or pear-shaped, and occupies the post-ocular region, extending from the posterior edge of the eye to the level of the corner of the mouth (Fig. 1). The posterior portion of the gland is rotated ventrally forming a posteroventral inflection of the VG. Although variable in size, we observed this inflection in all studied *Micrurus*, but it is absent in *Micruroides euryxanthus* (Fig. 1A, C, D, and G; Slowinski et al., 2001). In *M. narduccii*, we observed the most extreme posteroventral inflection of the VG, but in *M. spixii* the inflection was also very evident (Fig. 1C and D). The VG is constricted by the *adductor mandibularis externus superficialis muscle*, which attaches to the layer of connective tissue around its entire surface. Some muscle fibres follow the posterior curvature of the gland and are inserted into the surface of the posteroventral inflection of the gland (Fig. 1A, C, and D; Oliveira et al., 2021). The VG is constituted by large tubules that converge to the centre of the gland, but a central lumen is not observed (Fig. 1). The tubular aspect of the gland is better visualized in the sagittal sections (especially in Fig. 1D). The tubules are lined with columnar serous cells, with rounded basal nuclei (Fig. 1F). Secretory granules are present in the interior of cells, between their nuclei and apices, while the lumina of the acini show a high concentration of the secreted products, which is also clear in the sagittal sections (Fig. 1E and F).

The AG is also well-developed in all investigated coral snakes. This gland is contiguous with the VG proper and extends from the posterior level of the eye to the anterior portion of the maxilla, where it connects to the venom fang (Fig. 1). The accessory gland is composed of mucous acini constituted by prismatic cells. It can be differentiated from the VG in tomography images by the different shades of grey (Fig. 1B, C, D, and H). The VG and AG are surrounded by a contiguous layer of connective tissue and there is an abrupt histological change between the glands with an intermediary zone where the secretory tubules of the VG and acini of the AG are seen at the same level (Fig. 1). Although some hypotheses have been proposed regarding the biological function of the AG, such as contributing to the final composition of the venom (Valente et al., 2018), or to the chemical activation of the secreted venom, its true specific role in the venom system remains an enigma (Gans and Kochva, 1965; Rosenberg, 1967; Kardong, 2002; Mackessy and Baxter, 2006; Vonk et al., 2013). Our immunohistochemical analysis using a commercial anti-*Micrurus* antivenom as antibody in histological sections of the VG and AG of *M. corallinus* and *M. surinamensis* showed positive reactivity only in the VG region, indicating that the AG does not contribute significantly to the venom yield in these species (Fig. S1 in Supplementary file 3).

The morphology of elapid VGs has been described previously, especially for sea snakes and terrestrial elapids from Africa and Australia (Rosenberg, 1967; Burns and Pickwell, 1972; Halstead et al., 1978;

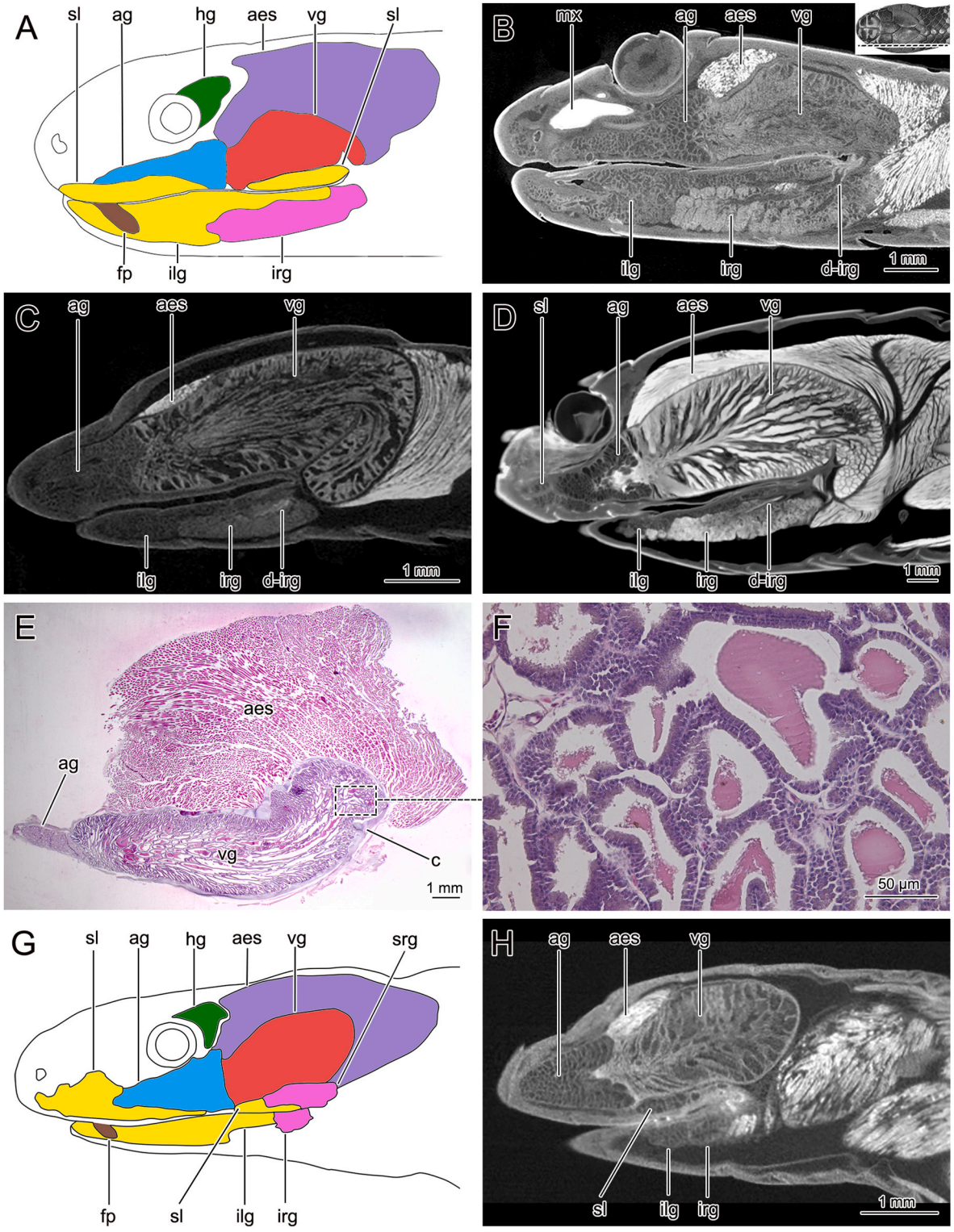

Fig. 1. Cephalic glands and associated structures in coralsnakes. (**A**) Schematic drawing of skinned head of *Micrurus'* species showing the location of the cephalic glands and the *adductor mandibulae externus superficialis* muscle (AES). Sagittal slices of high-resolution micro-CT scans of the heads of snakes showing the position of the venom gland (vg), accessory gland (ag), supralabial gland (sl), infralabial gland (il), inferior rictal gland (ir) and the muscle AES. The panel in the upper right corner of figure B denotes the position of sections B-F and H. (**B**) *Micrurus corallinus*, (**C**) *Micrurus narduccii*, and (**D**) *Micrurus spixii*. (**E**) Histological section of the venom apparatus of *Micrurus surinamensis* showing the venom gland, the muscle AES and the accessory gland (ag); staining = haematoxylin-eosin. (**F**) Detail of the anterior figure showing the acini of venom glands lined with prismatic cells and full of secretion; staining = haematoxylin-eosin. (**G**) Schematic drawing of the head of *Micruroides euryxanthus* showing the location of the cephalic glands and the muscle AES. (**H**) Sagittal slice of high-resolution computed tomography of the head of *Micruroides euryxanthus* showing the position of cephalic glands and the muscle AES. *Abbreviations*: c = connective tissue; d-ir = duct of the inferior rictal gland; fp = fang pocket; mx = maxillary; sr = superior rictal gland.

McCarthy, 1985; Gopalakrishnakone, 1986; Gopalakrishnakone and Kochva, 1990, Gopalakrishnakone and Kochva, 1993). However, only a small set of studies have addressed the VG of coral snakes, especially in species of the genus *Micrurus* (Rosenberg, 1967; Savitzky, 1979; Salomão, 1991; Giachi et al., 2007; Oliveira et al., 2021). Our results show that New World coral snakes display a well-developed VG and AG compared to the other elapids. Except for *Micruroides*, the VG of the New World coral snakes showed the posterior inflection of the gland. As previously discussed (Savitzky, 1979), among the thirteen investigated *Micrurus*, the extreme condition of the VG inflection was observed in *M. narduccii*. VG inflection is also observed in other elapids, such as *Bungarus*, *Laticauda*, and *Naja* (Rosenberg, 1967; Gopalakrishnakone and Kochva, 1990), but it seems to be particularly pronounced in *Micrurus*. Although the functional significance of this inflection is unknown, it may contribute to the increase in the size of the gland.

3.1.2. Molecular characterization

The three-finger toxin (3FTx) was the most expressed family of toxin in the VG for all four investigated species of *Micrurus* (Fig. 4, Table 1), corroborating previous findings (Leão et al., 2009; Corrêa-Netto et al., 2011; Aird et al., 2017). In *M. corallinus*, 3FTx accounted for 85.1% of toxin expression (59.4% of total transcriptome); in *M. tricolor*, 48.8% of toxin expression (32.9% of total transcriptome); in *M. lemniscatus*, 63.1% of toxin expression (37.6% of total transcriptome); and in *M. altirostris*, 71% of toxin expression (39.7% of total transcriptome) (Fig. 4, Tables S2–S5 in Supplementary file 1). *M. tricolor* differs from the other three species in 3FTx accounting for less than half of the toxin expression of the VG (Fig. 4), and a single 3FTx transcript represented about 25% of the total VG transcriptome (Table S3 in Supplementary file 1). Phospholipase A_2 (PLA_2) was the second most expressed family of toxins in *M. corallinus* and *M. tricolor*, accounting, respectively, for 9.2% of toxin expression (6.4% of total transcriptome) and 24.9% of toxin expression (16.8% of total transcriptome) (Fig. 4, Tables S2 and S3 in Supplementary file 1). In contrast, Aird et al. (2017) found the natriuretic peptide precursor (NP) as the second most abundant component in the venom of *M. corallinus*, representing more than 29.5% of the transcriptome of this species. Kunitz was the second most expressed family of toxins in *M. lemniscatus* (22.4% of toxin expression; 13.3% of total transcriptome) and *M. altirostris* (16% of toxin expression; 8.9% of total transcriptome) (Fig. 4, Tables S4 and S5 in Supplementary file 1).

The next most abundant venom component differed from venom to venom. In *M. corallinus*, NP precursor was the third most abundant component, representing 1.8% of toxin expression (1.3% of the total transcriptome) (Fig. 4, Table S2 in Supplementary file 1). In addition to 3FTx and PLA_2, the most abundant component of *M. tricolor* was Kunitz, which accounted for 22.7% of toxin expression (15.3% of the total transcriptome). In both *M. lemniscatus* and *M. altirostris*, PLA_2 was the next most abundant component of the venom. In *M. lemniscatus*, PLA_2 accounted for 11.5% of toxin expression (6.8% of the total transcriptome), whereas in *M. altirostris*, PLA_2 accounted for 8.5% of toxin expression (4.7% of the total transcriptome) (Fig. 4, Tables S4 and S5 in Supplementary file 1). In addition to these highly expressed toxins, all VG transcriptomes recovered minor components, such as C-type lectin (CTL) and other lowly expressed toxins (Fig. 4, Tables S2–S5 in Supplementary file 1).

Proteomic analyses identified most of the toxins recognized from their transcripts. In the *M. corallinus*, 19 venom proteins belonging to nine protein families were identified (Table S6 in Supplementary file 1). The 3FTx and PLA_2 were the most abundant toxins (respectively, 25.3% and 8.2% of the total VG proteome). Kunitz and NP were not identified in the proteome of this species. In contrast, snake venom metalloproteinases (SVMP), CTL, and L-amino acid oxidases (LAO) were seen in proportionally higher numbers in the proteome than in the transcriptomes (Table S6 in Supplementary file 1). In *M. tricolor*, 27 venom proteins belonging to eight proteins families were identified, with the PLA_2 (31.9% of the total VG proteome) being the most abundant, followed by 3FTx (19.1%) and Kunitz (9.7%) (Table S7 in Supplementary file 1). In *M. lemniscatus*, 25 venom proteins belonging to eleven protein families were identified (Table S8 in Supplementary file 1). Although 3FTx and PLA_2 were the two families most relevant in terms of number of proteins (6 and 5, respectively), PLA_2 was the most abundant toxin, accounting for 12.9% of the total VG proteome. 3FTx accounted for only 3.2% of the total proteome, a proportion much lower than that observed in the transcriptome. Differently, LAO, ohanin-like (OHAN), and SVMP were higher observed in the proteome than in the transcriptome (Table S8 in Supplementary file 1).

The correlation between the transcriptomic and proteomic abundance of venom is variable within the species. Although some studies have shown similar results in both analyses (Corrêa-Netto et al., 2011; Aird et al., 2013; Yin et al., 2020; Modahl et al., 2021), discrepancies in transcriptomic and proteomic abundances may be expected as a consequence of using a species consensus VG transcriptome instead of an individual VG transcriptome to perform the proteomic analysis (Rokyta et al., 2015; Hofmann et al., 2018; Nachtigall et al., 2022). Moreover, a study with micrurine snakes showed extremely poor quantitative correspondence between transcriptomes and proteomes (Aird et al., 2017), which indicates that 3FTx is especially problematic in that their estimated abundance tended to be drastically lower in the proteomes than transcriptomes, probably due to its inherent low potential of generating ionized tryptic peptides in mass spectrometry. In this study, we had transcriptomes and proteomes obtained from the same specimens only for *M. tricolor*. Although for this species the largest number of venom proteins was recovered, the quantitative correspondence between transcriptomes and proteomes was modest. 3FTx was quantitatively less represented in the proteome than in transcriptome, which corroborates to the finding that estimating abundance is problematic (Aird et al., 2017). The weaker correspondence between transcriptomes and proteomes in *M. tricolor* and *M. lemniscatus* suggests that posttranscriptional regulatory mechanisms may be shaping the number of final toxins proteins produced by these species and indicates that the relationship between the two approaches to studying the venom profile needs to be better investigated in future studies.

In summary, despite the species investigated and the differences between gene expression and mature protein availability in the venom, the venoms from the representative species studied here indicate that three protein families (3FTx, PLA_2, and Kunitz) constitute the major constituents of *Micrurus* venoms, whereas several other proteins should be ancillary players in the venom. Generally, our results agree with the previous investigations of *Micrurus* species (Corrêa-Netto et al., 2011; Lomonte et al., 2016; Aird et al., 2017), while the main difference observed is related to the venom composition of the *M. corallinus*. Whereas some previous studies have shown the predominance of 3FTx and PLA_2 (Corrêa-Netto et al., 2011), as observed here, other studies have demonstrated higher amounts of NP (Aird et al., 2017), suggesting intraspecific and/or geographical variation in the composition of the venom. The venom of *M. tricolor* differs from the other species investigated here by having the lowest amount of 3FTx. This species is little known in terms of biology and phylogenetic relationships, but a difference in the venom composition can be observed even between it and *M. altirostris*, two species of the triad-banded species group and supposedly closely related phylogenetically (Silva Jr et al., 2021b).

3.2. Inferior rictal and infralabial glands

3.2.1. Morphology

Here, we report that all New World coral snakes investigated have two distinct glands in the mandibular region, the ILG and an inferior RG (Figs. 1 and 2). These two glands can be differentiated by the topology and format of their acinar structures. The ILG is located just below the infralabial scales extending from the anterior to the posterior part of the mouth, while the inferior RG is located more ventrally extending from the medial part of the mandible to the corner of the mouth (Figs. 1 and

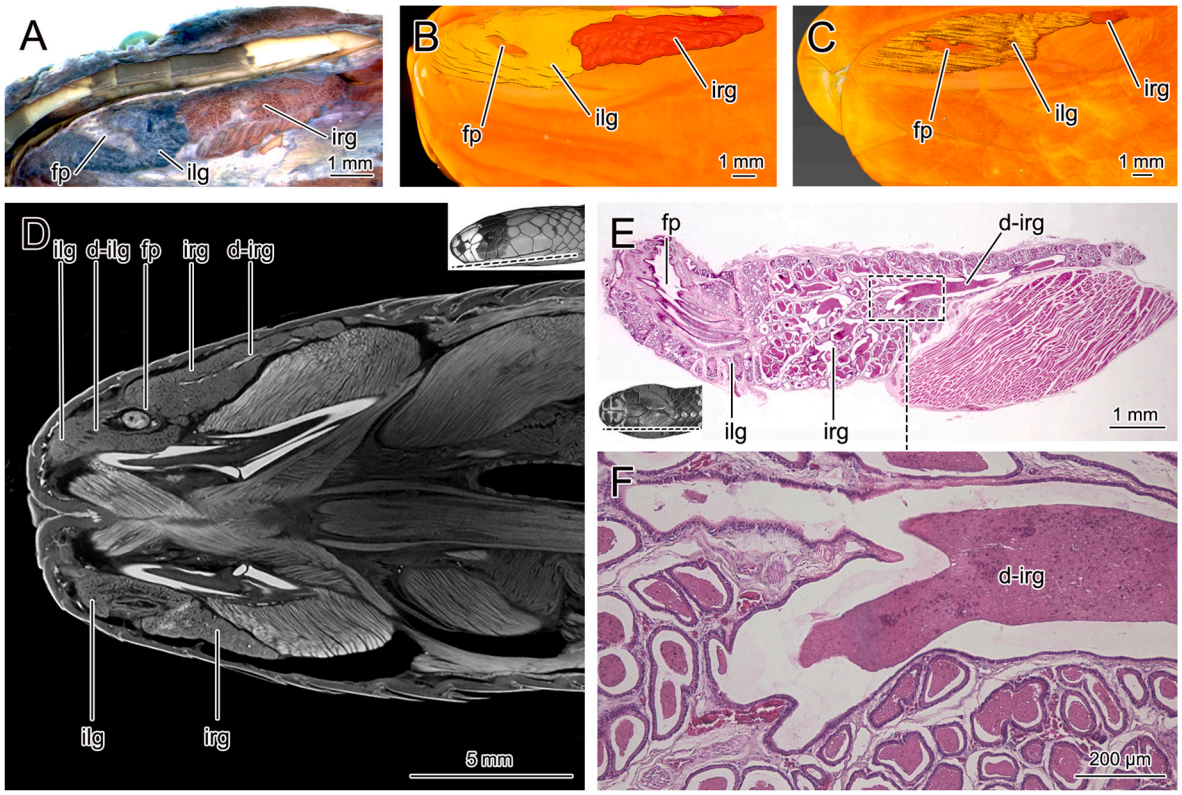

Fig. 2. Lower jaw glands in coralsnakes. (**A**) Photograph of the skinned head of *Micrurus lemniscatus* showing the location of the infralabial gland (il), fang pocket (fg) and the inferior rictal gland (ir). Segmented reconstruction of high-resolution computed tomography of the lower jaw showing infralabial gland, fang pocket and inferior rictal gland in *Micrurus corallinus* (**B**) and *Micruroides euryxanthus* (**C**). (**D**) Frontal slice of high-resolution computed tomography of the head of *Micrurus surinamensis* showing the position of infralabial gland, fang pocket, inferior rictal gland and the duct of the inferior rictal gland (d-ir) distending to the region of the corner of the mouth. The panel in the upper right corner of the figure denotes the position of section. (**E**) Sagittal section of the glands of *Micrurus surinamensis* showing the acini of the infralabial gland, the fang pocket, the acini of the inferior rictal gland and the duct of the inferior rictal gland full of secretion and distending to the posterior portion of the mouth; staining = haematoxylin-eosin. The panel in the lower left corner of the figure denotes the position of section. (**F**) Detail of anterior figure showing the acini and duct of the inferior rictal gland; staining = haematoxylin-eosin.

2). In *Micruroides euryxanthus* the inferior RG is tiny, occupying only the posterior-most region of the mandible (Figs. 1 and 2) whereas in all other studied *Micrurus*, it is larger and occupies the posterior halves of the mandibles under the infralabial scales. At the level of the fangs, the ILG is covered by the oral epithelium which divides the gland laterally into two portions (Figs. 1 and 2). This organisation is present in all studied elapids and is associated with the region where the fangs are accommodated in the mandible when the snake's mouth is closed: a "fang pocket" (Kochva, 1978; Oliveira et al., 2021). The ILG is constituted of mucous cells, as evidenced by the positive reactivity to alcian blue (Fig. 2A), but some serous cells can also be observed in this gland. The ILG shows several short ducts that open along the mandible in the contact between infralabial scales and the oral epithelium, although in the region of the fang pocket some ducts are most elongated and directed to the anterior part of the mouth (Fig. 2D; Oliveira et al., 2021). There is no evidence of the duct from the ILG opening into the fang pocket. Inferior RGs are constituted exclusively by serous cells arranged in more voluminous and full secretion acini (Fig. 2E and F). This gland also shows a single duct that extends posteriorly from the central region of the gland and opens in the corner of the mouth (Fig. 1B–D and Fig. 2D–F). As with acini, RG ducts are full of secretions (Fig. 2E and F). As exceptions, the RG duct of *M. surinamensis* consists of serous cells (Fig. 2F), whereas that of *M. lemniscatus* is composed of mucous cells (Oliveira et al., 2021). We found a small superior RG in *Micruroides euryxanthus* (Fig. 1G), *Micrurus narduccii*, *M. frontalis* and *M. spixii*. Like the inferior RG, the superior RG also empties via a single duct opening in the corner of the mouth (results not shown).

Our results improve our understanding of morphological traits of the inferior RG in New World coral snakes and reveal a superior RG with morphological variations, which is small but well-developed in *Micruroides euryxanthus*. Underwood (1997) first recorded a RG in the elapids, while Wollberg et al. (1998) focused their observations on RGs in Atractaspididae snakes compared to some viperids and elapids. In the elapids, Wollberg et al. (1998) found evidence of the superior RG and no evidence of an inferior RG in *Aspidelaps scutatus*, *A. lubricus*, *Elapsoidea guentheri* and *E. sundevalli*. In *Bungarus flaviceps*, *Naja mossambica*, *Ophiophagus hannah* and *Walterinnesia aegyptia*, the authors did not find evidence of any RG. Moreover, the most conspicuous RGs in elapids was observed in *Naja multifasciata*, which possesses both superior and inferior RG, but differently from New World coral snakes, the superior RG is larger than the inferior (Underwood, 1997). A similar condition is also observed in the atractaspidids, where most species possess both superior and inferior RG and the superior glands are frequently better developed (Wollberg et al., 1998). Recently, Jackson et al. (2017) expanded our knowledge of RGs in elapids with a survey of the macroscopic anatomy of these glands in several species of the family, but neither the inferior RG nor the shape or size of the superior RG were addressed. Among the Old World coral snakes, a single report shows that *Calliophis castoe* has an ILG with distinct anterior and posterior regions (Smith et al., 2012). Although no RG has been formally described for these snakes to date, this report suggests that the posterior area of the ILG is an inferior RG, indicating that the RG is more widely distributed in elapid snakes than previously thought. Furthermore, the persistence of RG in many snake lineages suggests that this gland may have important functional roles (Wollberg et al., 1998), especially in *Micrurus* species that have a well-developed inferior RG.

Despite consisting mostly of serous cells and being present in multiple species, studies focusing on understanding the biological roles of RGs are still scarce (McDowell, 1986; Underwood, 1997, 2002; Jackson et al., 2017; Oliveira and Zaher, 2022). These studies suggest that RGs are associated with antimicrobial activity, lubrication and/or venom production (Jackson et al., 2017). In the non-caenophidian snakes, one report showed some toxicity of RG secretions in Erycinae and Uropeltidae (Phisalix and Caius, 1918). In *Cylindrophis ruffus*, the RG expresses typical toxin genes which are also present in other mandibular and maxillary glands (i.e., infra- and supralabial glands) of the species, and it is hypothesized that these glands may share a similar ontogenetic developmental program and evolutionary history (Fry et al., 2013).

ILGs are present in all snakes studied so far but, like with RGs, only a few studies addressed their biological roles (Smith and Bellairs, 1947; Taub, 1966; Kochva, 1978). Most ILGs are constituted by mucous cells, and it is hypothesized that this gland may be mainly associated with the lubrication of the mouth (Kochva, 1978; Oliveira et al., 2008; Jackson et al., 2017). One study showed that this ILGs may represent an auxiliary source of toxins in some non-caenophidian species (Fry et al., 2013), but no study has performed protein characterization to corroborate these findings. In elapids, one report that injected secreted proteins from ILG of *Micrurus nigrocinctus* produced symptoms of envenomation in mice (Dix, 1978). Dix (1978) did not recognize the existence of two distinct glands in the mandible but reported the ILG to be divided into lateral and medial portions releasing secretions into the snake's mouth independently. Our observations suggest that Dix's divisions of the ILG represent in fact the ILG and RG. Thus, this work may represent the first evidence about the function of the inferior RG and ILG in a caenophidian snake. Additionally, further studies reported for the RG and ILG of the non-caenophidian species (i.e., Phisalix and Caius, 1918; Fry et al., 2013) constitute the very limited information available on the function of these glands in snakes.

3.2.2. Molecular characterization

To gain insights about the functions of the ILG and RG in micrurine species, we surveyed the gene expression in these glands through a transcriptomic analysis, complemented by a proteomic validation of proteins present in gland extracts. First, we looked for possible signs of toxin production in these glands and further characterized other non-toxin products highly expressed there.

We recovered several toxin families in the transcriptomes of inferior RGs and ILGs (Fig. 4, Table 1) but these toxin transcripts were detected at low to medium levels. In *M. corallinus* and *M. tricolor*, the ILG shows a higher level of expression of CTL than RG, corresponding, respectively, to 81.1% and 93.4% of the toxin expression (respectively, 12.7% and 8.5% of the total transcriptome) (Fig. 4, Tables S2 and S3 in Supplementary file 1). In the RG, CTL corresponded to 73.7% of toxin expression (4.6% of the total transcriptome) of *M. corallinus* and 58.5% of toxin expression (2.8% of the total transcriptome) of *M. tricolor*. Differently, in *M. tricolor*, 3FTx, the second most expressed toxin of this species, was more expressed in the RG than in the ILG. In *M. lemniscatus*, although the RG showed a higher level of expression of SVMP and CTL than ILG, when observed the total transcriptome (Table S4 in Supplementary file 1), the general proportion between these two families of toxins was similar in the two glands. In *M. altirostris*, CTL was also the most abundant family of toxins in the ILG, representing 84.2% of the toxin expression (5.1% of the total transcriptome), but for this species we have no information about RG.

The presence of different toxin families in the RG and ILG of micrurine snakes agrees with the previously observed in non-caenophidian snakes (e.g., Fry et al., 2013), which indicates that these glands have several functional roles not only lubrication. However, the dominance and level of expression of these toxins were very different from those observed in the VG. The 3FTx, the most expressed toxin family in the four studied micrurine VG and often highly expressed in the venom of elapids (Fig. 4; Jiang et al., 2011; Lomonte et al., 2016; Dashevsky et al., 2021), was invariably present in RG and ILG transcriptomes, but in general represented less than 1% of the total transcripts. Only in the RG of *M. tricolor*, the proportion was higher (1.7%). In this species, we also found a significant difference in expression levels between the two individuals. In one individual, 3FTx represented 3.5% of the total transcriptome, while it represented 0.02% in another (Table S3 in Supplementary file 1). The other two families of toxins well-represented in the VG transcriptomes, PLA_2 and Kunitz, did not exceed 1% of RG and ILG transcriptomes (Table S3 in Supplementary file 1).

In contrast, RGs and ILGs showed levels of expression of CTL, cysteine-rich secretory protein (CRISP) and SVMP comparatively higher than in VGs (Fig. 4, Tables S2–S5 in Supplementary file 1). CTL has been previously reported for many *Micrurus* venoms and exhibit tremendous sequence variation in these snakes, but in general they are considered minor toxins in Elapidae, representing between 0.1% and 2.0% of the toxin transcriptome (Corrêa-Netto et al., 2011; Aird et al., 2017; Sanz et al., 2019). Our sequences of CTL recovered from RGs and ILGs exhibited high identity with the typical micrurine CTL from the VG transcriptomes, but with exception of those of *M. tricolor* they were not clustered with the more expressed CTL from the VG in our phylogenetic analysis (Fig. S2 in Supplementary file 3), indicating that RG and ILG CTLs are different from the typical CTL found on *Micrurus* venoms. However, predicted signal peptides have been found in all CTL of the investigated species and we recognize a greater abundance of CTL in the proteomes of RG and ILG (Tables S6–S8 in Supplementary file 1). Although CTL has not been pharmacologically characterized to date for any *Micrurus* species and little is known about its function (Aird et al., 2017; Rincon-Filho et al., 2020), the higher quantities of CTL in RGs and ILGs than in VGs indicate it has some enigmatic functional importance for these glands and snakes.

In *M. corallinus*, SVMP corresponded to 10.5% of the toxin expression (0.65% of the total transcriptome) of the RG and 2.5% of toxin expression (0.39% of the total transcriptome) of the ILG (Fig. 4, Table S2 in Supplementary file 1). At least four transcripts of SVMP were recognized in the RG and ILG of *M. corallinus*, but only in the ILG, SVMP was recovered in the proteome (Table S6 in Supplementary file 1). Additionally, as with 3FTx, high individual variation was seen in the expression of SVMP in the RG, where the expression varied from 0.0002% of the total transcriptome in one individual to 1.93% of the total transcriptome in another (Table S2 in Supplementary file 1). In *M. lemniscatus*, four transcripts of SVMP were recognized in the RG and three in the ILG, totalling 19.6% of the toxin expression (2.03% of the total transcriptome) of RG and 13.6% of toxin expression (1.02% of the total transcriptome) of the ILG (Fig. 4, Table S4 in Supplementary file 1). Like the CTL, the SVMP most expressed in RGs and ILGs were not the same as those most expressed in VGs.

Individual variation in the expression level of toxins suggests that, as with VGs, the secretory profile of RGs and ILGs may be influenced by individual factors, such as ontogenetic or sexual differences (Amorin et al., 2018; Braga et al., 2020; Freitas-de-Sousa et al., 2020). Unlike VGs, for which secretory cycle is relatively well-known and protein synthesis is stimulated by venom extraction, the secretory cycle and mechanisms of RGs and ILGs are unknown. These glands do not have compressor musculature or connection with maxillary teeth, which makes any attempt to empty these glands by manual stimulation unpredictable. Consequently, the gland extraction could not be used as stimuli for protein synthesis. Thus, it is possible that substantially different levels of protein synthesis are present in RGs and ILGs, which may also explain the high differences in the expression level of some toxins between the individuals of the same species. It is important to emphasize that the preparations and the NGS sequencing of ILG and RG transcriptomes were performed independently from those of the VGs, i.e., the RNA was not extracted at the same moment as that from the VG, the libraries were not prepared together, and the ILG and RG libraries were not pooled on the same instrument run containing VG libraries. So,

the low expression of toxins in ILGs and RGs can be ruled out as a contamination from VG and indeed represents residual gene expression on these glands.

Studying snake venom evolution by leveraging the complete genome of the Burmese python (*Python bivittatus*), Reyes-Velasco et al. (2015) observed high expression of 3FTx and CTL orthologous genes in the RG, which is consistent with our results and previous reports in the non-caenophidian snakes (Fry et al., 2013). However, authors also demonstrated the expression of other venom gene homologs at comparable levels in many other tissues, such as the brain, liver, and intestinal tissue and suggested that, in the absence of functional activity data, caution is required when attempting to extrapolate from protein toxin family identification to biological activity (Reyes-Velasco et al., 2015). In elapids, the only experimental evidence on the function of RGs and ILGs comes from Dix (1978), who demonstrated that the extract from these two glandular regions (ILG and inferior RG) was toxic to mice when injected intraperitoneally, causing the characteristic symptoms of the coral snake envenomation. However, since then, these mandibular glands of *Micrurus* have never been studied in terms of protein characterization or functional activity. Building on Dix's report, Roze (1996) suggested that the secretions produced by the glands could be conducted by the grooved teeth of the dentary that are found in *Micrurus* and other elapids (Young and Kardong, 1996; Oliveira et al., 2021). Although we did not observe a relationship between the ducts of the glands and the teeth in the dentary, we cannot discard the possibility that these grooves in dentary teeth could help conducting secretions produced by RGs and ILGs. Additionally, although we obtained negative recognition of venom in immunohistochemistry experiments using anti-*Micrurus* antivenom (Fig. S1 in Supplementary file 3), our transcriptomic and proteomic findings, show that both glands can produce small levels of toxins or toxin-like proteins, especially an exclusive type of CTL, which may explain the toxic effect of the extract of these glands in mice.

Most RG and ILG transcriptomes were constituted by nontoxin components (Fig. 4, Tables S2–S5 in Supplementary file 1). Ficolins represented the most expressed transcripts of both glands in all studied species (Tables S2 and S3 in Supplementary file 2). Ficolins constitute a class of non-enzymatic components found in the transcriptomes of VG of several snake species, including *Micrurus altirostris* and *M. corallinus* (Corrêa-Netto et al., 2011; Fry et al., 2012; Junqueira-de-Azevedo et al., 2016; Modahl et al., 2018; Viala et al., 2015), but its toxicity and function is unknown in snakes. In mammals, ficolins have been associated with the innate immune response throughout the circulation and within organs, recognizing and removing numerous bacterial, viral, fungal, and parasitic pathogens (Bidula et al., 2019). Venom ficolins (veficolins) were found in the venom proteome and the VG transcriptome of the homolopsid *Cerberus rynchops* and have been classified as a putative class of toxins (Ompraba et al., 2010). Based on its structural similarity to ficolin, authors speculate that veficolins may induce platelet aggregation and/or initiate complement activation, but its toxic activity in the venom is unknown (Fry et al., 2012). In the RG and ILG of the investigated micrurine species, the recovered ficolin transcripts present low similarity to the veficolins of *C. rynchops*; however, these recovered ficolins present a signal peptide and are identified in the tissue proteomes (Tables S2 and S3 in Supplementary file 2), which suggests important roles for these ficolins in the species investigated.

Other nontoxin transcripts that are among the highly expressed genes in RGs and ILGs are two enzymatic components cholinesterase and chitotriosidase (Tables S2 and S3 in Supplementary file 2). Sequences of cholinesterase from RG and ILG were most like those of the elapids *Pseudonaja textilis* and *Notechis scutatus*, but some also showed high similarity with the acetylcholinesterase from the colubrid *Boiga irregularis* (Pla et al., 2018). Acetylcholinesterase is a type of cholinesterase present in the venom of diverse species of snakes, particularly from the family Elapidae (Fry, 2005; Ahmed et al., 2010; Aird et al., 2017). According to Aird et al. (2017), micrurine acetylcholinesterases are highly variable in the primary structure and, in *M. lemniscatus*, where they were more abundant, they represent 0.05% of the VG transcriptome, a number lower than that observed here for ILGs and RGs. Although little is known about its function in the venom, it was suggested that acetylcholinesterase facilitate prey capture, having a functional role in catalysing the hydrolysis of acetylcholine in muscles (Ahmed et al., 2010). However, occurrence of this enzyme in ILG/RGs at higher levels than in VGs, may indicate that its role in the oral cavity is unrelated to the envenoming of prey.

Searches of our transcriptome sequences revealed chitotriosidase from RGs and ILGs, showing highest identity with those of the elapids *Notechis scutatus* and *Pseudonaja textilis*. Chitotriosidase or chitinase are enzymes poorly known for the cephalic glands of snakes, but they have been found in the oral glands of some Anguimorpha lizards (Koludarov et al., 2017). In mammals, chitotriosidases are mainly produced by activated macrophages and epithelial cells and are capable of hydrolysing chitin. They are associated with the defence against pathogens by playing roles as a host defence towards chitin in pathogen's cell structure and any dysregulation in its expression level may lead to several diseases, such as bronchial asthma and atherosclerosis (Kanneganti et al., 2013). These enzymes may also play a role in digestion of arthropods (Hamid et al., 2013). However, unlike the anguimorpha lizards, which include arthropods in their diet, the diet of *Micrurus* consists mainly of vertebrates (e.g., fossorial snakes, amphisbaenians and caecilians), with few species feeding on invertebrates (e.g., *M. hemprichii*, which also feeds on onychophorans) (Marques and Sazima, 2021). Thus, a defence-associated function for chitotriosidase seems more likely for these snakes than a chitin digestion function.

Other highly expressed nontoxin RG and ILG transcript code for immunoglobulins (Tables S2 and S3 in Supplementary file 2). The high level of expression of the immunoglobulins agrees with the hypothesis that the secretion of these glands may be associated with some type of antimicrobial activity and immune response (Jackson et al., 2017).

Although RGs and ILGs are distinct morphologically, their gene expression profiles were revealed to be quite similar in our analysis, as evidenced by Fig. 5 and Table 1. The similarity in expression profiles may indicate a similar biological role for both glands, which may be acting together to complement their functions. However, we may not discard the possibility of having both glands not completely dissociated during the dissection. The dissection process was performed with severe caution, but the proximity of both glands and the high similarity between them when unstained may have led to some degree of contamination. Further studies focusing on performing single-cell and/or cell-sorting transcriptomic methodologies may help confirm the results obtained in this study.

Proteomic data from RGs and ILGs agrees with the transcriptome data (Table S7 in Supplementary file 1 and Tables S2 and S3 in Supplementary file 2) in that we identified most families of proteins encoded by toxins and nontoxins components recovered in the transcriptome. Among the toxin transcripts, which represented only 7% of the proteome of the RG of *M. tricolor*, the highly expressed protein family of toxins was CTL (2.4% of the proteome), followed by 3FTx (2.0% of the proteome) (Table S7 in Supplementary file 1). The nontoxins account for 93.1% of the proteome of this gland. Ficolin was the most expressed protein, with at least three different proteins among the top-30, accounting for 8.3% of the proteome. Other highly abundant proteins in RGs were immunoglobulin (2.1%), and chitotriosidase (1.2%) (Table S7 in Supplementary file 1 and Table S2 in Supplementary file 2). In the ILG of *M. tricolor*, the most expressed protein family of toxins was CTL, totalling 5.3% of the proteome. PLA_2 was the second most expressed family of toxins, representing 0.5% of the glandular proteome (Table S7 in Supplementary file 1). Nontoxin proteins account for 93% of the glandular proteome of this gland. The immunoglobulin, ficolin and chitotriosidase are also among the most expressed proteins of this gland (Table S3 in Supplementary file 2).

3.3. Harderian glands

3.3.1. Morphology

HGs are well-developed and confined to the orbit in all species examined (Fig. 1A, G, and Fig. 3). Only a small portion of the HG is observed between the posterior surface of the eye and the *adductor mandibularis externus superficialis* muscle in skinned heads (Fig. 1A, G), but this gland may exceed the eye in size and occupies an extensive proportion of the area between the lateral surface of the frontal bone and the medial surface of the eye (Fig. 3). We reconstructed a 3D model of the HG for *Micrurus surinamensis* to better visualize their segmented structures and show that their anterior regions are connected to the nasolacrimal duct (Fig. 3). At the end of this connection, the nasolacrimal duct turns medially and then posteriorly to reach the medial portion of the duct of the vomeronasal organ (VNO) (Fig. 3). The tortuous course of the nasolacrimal duct is better visualized in the 3D model (Fig. 3), while only a limited extent of the duct can be seen in the histological sections (Fig. 3E). In *M. corallinus*, the HG is composed of serous cells with rounded basal nuclei arranged in acini with reduced lumina, and by ducts that are more abundant in the glandular portion located in the medial surface of the orbit (Fig. 3D). HG ducts are lined by mucous cells and there is no evidence of any HG duct opening in the orbital space (Fig. 3D).

Savitzky (1979) described HGs of several micrurine species and mentioned variability in relative size despite a highly conserved shape. He also noted that the shape of the exposed part of the gland may be broad (e.g., *M. corallinus* and *Micruroides*), elongated and acute (e.g., *M. filiformis* and *M. narduccii*), or tiny (e.g., *M. surinamensis*). Our micro-CT scan data evidenced that HG shape is conserved among all fourteen species studied, as can be observed in *M. surinamensis* (Fig. 3).

Although HGs are frequently confined to the orbit in elapids, they extend beyond the orbit in the long-glanded, Old World coral snakes of the genus *Calliophis* (McCarthy, 1985; McDowell, 1986; Slowinski et al., 2001) which have an expansion of the posterior extension of the HG (Slowinski et al., 2001; Brown et al., 2018). The association between fibres of the *adductor mandibularis externus superficialis* muscle and the posterior and medial surfaces of the HG is also observed in some species of *Calliophis* (Slowinski et al., 2001; McDowell, 1986:373; Brown et al., 2018). HGs that are not confined to the orbit is a widespread condition in non-elapids (McCarthy, 1985), but there is also a relationship between HG development with fossoriality and cryptozoic habits in snakes, as well as a relationship between decreased eye size in snakes with increasing HG (Savitzky, 1979). Large HGs have been described also in the egg-eating snakes, such as *Dasypeltis* and *Elachistodon* and in the goo-eating dipsadines, where these glands extend far beyond the back of the eyes (Smith and Bellairs, 1947; Oliveira et al., 2014; Zaher et al., 2014). No hypothesis to explain the selective forces leading to the enlargement of the HG have yet been proposed.

Although not usually considered an oral gland, HGs indirectly connect to the oral cavity via the nasolacrimal duct, which discharges on the posteromedial surface of the VNO duct (Bellairs and Boyd, 1947, 1949; Taub, 1966; Burns and Pickwell, 1972; Rehorek et al., 2003). In both pygopodid geckos and in snakes, in which the eyelids have fused to form a transparent spectacle, the HG duct opens directly into the nasolacrimal

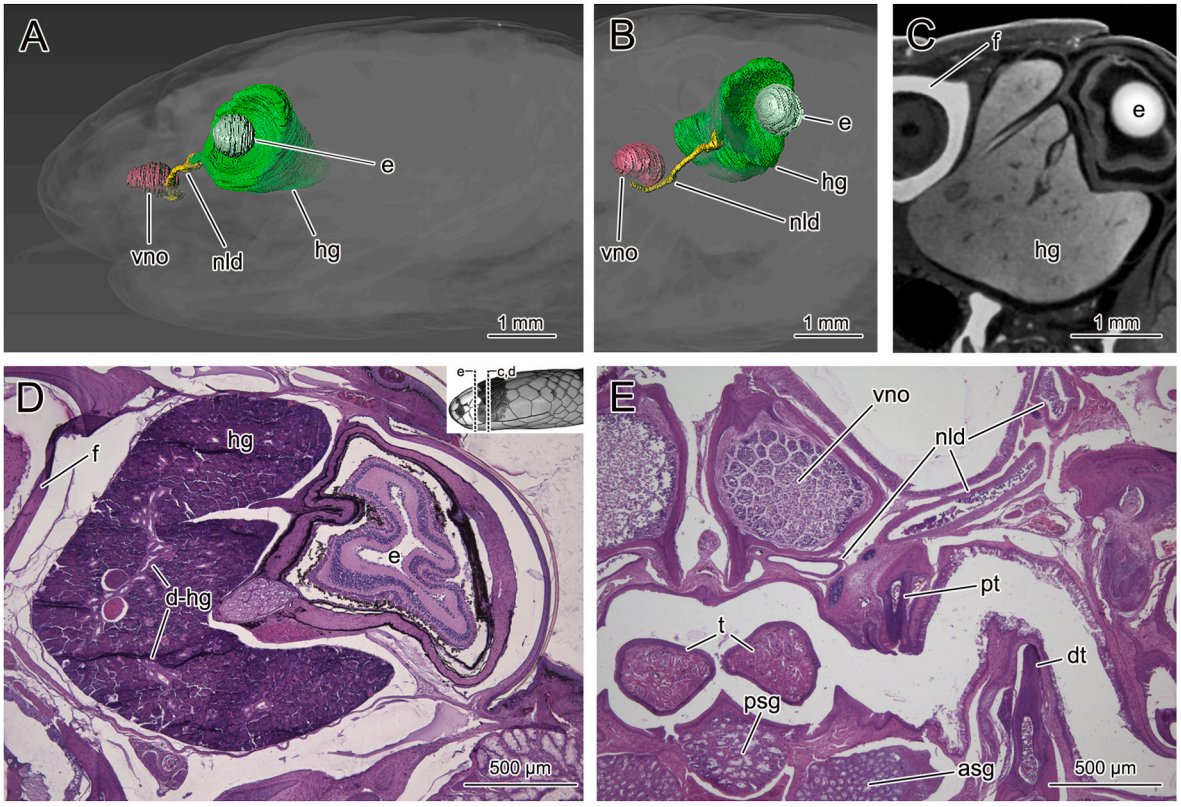

Fig. 3. Harderian glands and associated structures in coralsnakes. (**A**) Segmented reconstruction of high-resolution computed tomography of the head of *Micrurus surinamensis* showing the lateral view of Harderian gland and its connection with the vomeronasal organ (vno) via the nasolacrimal duct (nld). (**B**) Lateromedial view of the anterior figure showing the position of the Harderian gland and the tortuous nasolacrimal duct that opens on the posteromedial surface of the vomeronasal organ. (**C**) Transversal slice of high-resolution computed tomography showing the position of the Harderian gland between the lateral surface of the frontal (f) and medial surface of the eye (e). (**D**) Transversal section of the head of *Micrurus corallinus* showing the Harderian gland with its mucous ducts (d-hg); staining = haematoxylin-eosin. The panel in the upper right corner of the figure denotes the position of sections C, D and E. (**E**) Transversal section of the head of *Micrurus corallinus* showing the nasolacrimal duct directed toward the posteromedial surface of the vomeronasal organ; staining = haematoxylin-eosin. *Abbreviations*: asg = anterior sublingual gland; dt = dentary tooth; psg = posterior sublingual gland; pt = pterygoid tooth; t = tongue.

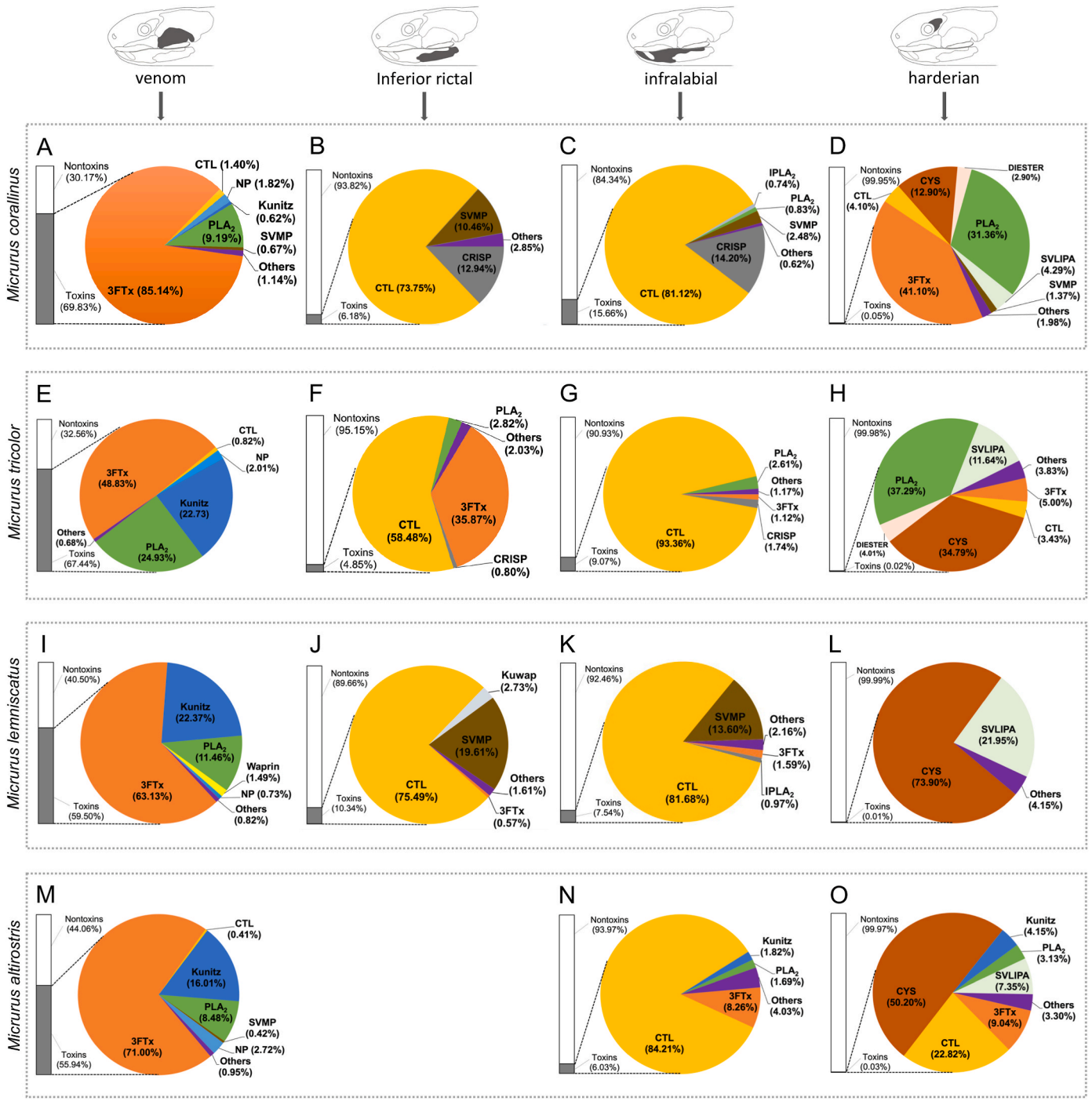

Fig. 4. Pie charts of the proportion of total transcripts per million (TPM) accounted for the major toxin families identified in the transcriptomes of the venom, inferior rictal, infralabial and Harderian glands. Pie charts columns represent the different glands and the rows of the different species studied. The bars on the left side of the pie charts represent the proportion of toxins and nontoxins transcripts to the total transcriptome of the glands. The figures at the top of each column indicate the topographic position of the different glands in the heads of the snakes. Data are the average of different numbers of individuals for species or glands (see Tables S2–S5 in Supplemental file 1 for individual data).

duct and completely bypasses the conjunctival space (Hillenius and Rehorek, 2005). In non-caenophidian snakes, the nasolacrimal duct itself still opens into the conjunctival space, whereas in most caenophidians (e.g., Colubridae, Elapidae, Viperidae) this connection is vestigial, and the nasolacrimal duct conveys HG secretions almost exclusively (Smith and Bellairs, 1947; Hillenius and Rehorek, 2005). Our morphological investigation of the micrurine snakes confirm the existence of a connection between HG and VNO through a nasolacrimal duct (Fig. 3).

The function of HG in snakes has not been clarified experimentally, but these glands have been associated with orbital lubrication and chemosensory/vomerolfaction, transferring chemical signals, such as female pheromones and feeding cues to the VNO sensory epithelium (Saint-Girons, 1982, 1988; Rehorek, 1997; Rehorek et al., 2000a; Souza et al., 2015; Dominguéz-Peréz et al., 2019). It is due to the connection via the nasolacrimal duct and to the fact that although the VNO is morphologically and chemically like the olfactory organs, no intrinsic lubrification is associated with this organ (Hillenius and Rehorek, 2005).

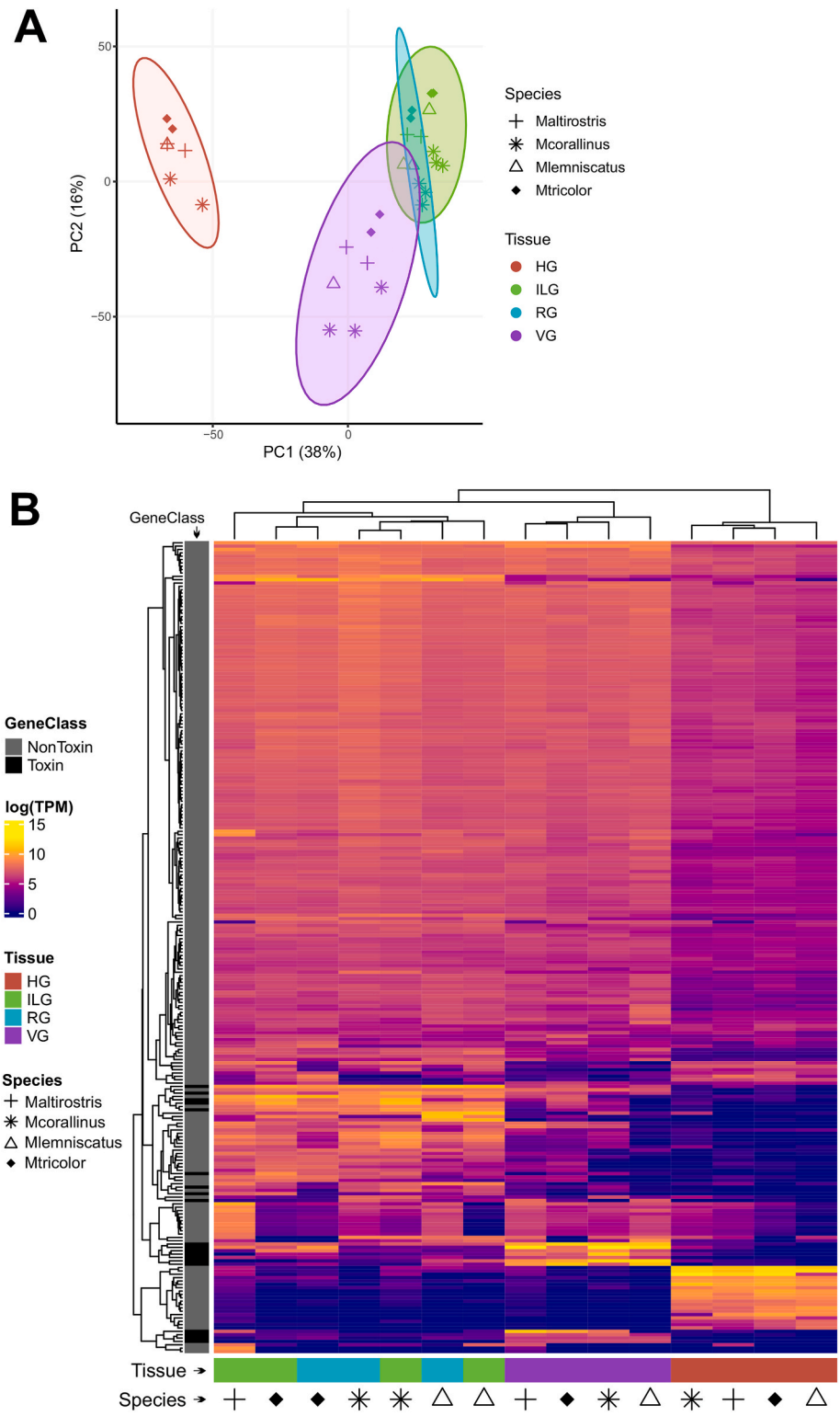

Fig. 5. Expression pattern of orthologs among cephalic glands in the *Micrurus* species studied. **(A)** Principal component analysis (PCA) showing the similarity and differences of orthology expression among glands. Ellipses represent 95% confidence intervals. **(B)** Heatmap of the top 150 highly expressed genes in each gland with a hierarchical clustering of glands based on expression level of orthologs revealing a similar clustering to that observed in the PCA.

Thus, the HG appears the main candidate to supply the extrinsic secretion to VNO (Rehorek et al., 2000b).

3.3.2. *Molecular characterization*

The HG showed the lowest level of toxin RNA expression among all glands investigated, with total toxin transcripts representing less than 0.1% of the gland transcriptome (Fig. 4, Tables S2–S5 Supplementary file 1). In *M. corallinus*, the most expressed putative toxin family was 3FTx, representing 41.1% of the toxin expression (0.02% of the total transcriptome). In *Micrurus tricolor*, the most expressed putative toxin family was PLA_2, representing 37.3% of the toxin expression (0.01% of the total transcriptome), whereas in *M. lemniscatus* and *M. altirostris*, the

most expressed putative toxin family was cystatin (CYS), representing, respectively, 73.9% and 50.2% of the toxin expression and 0.01% of the total transcriptomes of each species (Fig. 4). Other trace levels of the putative families of toxins were observed in the HG of all studied species (Fig. 4, Tables S2–S5 Supplementary file 1).

The proteomic data revealed a slightly higher proportion of toxins than observed in transcriptomes (Tables S6–S8 in Supplementary file 1). However, it is possible the toxin families in HG proteomes are minor contaminants. Due to their anatomical position, HGs were harvested from only after dissection of the VG, with the potential for venom proteins released from VGs or oral cavity contaminating adjacent tissues, and this might explain the higher level of venom proteins in HG proteomes compared with transcriptomes. Accordingly, the families of toxins observed in HG proteomes, particularly 3FTx and PLA_2, are the ones highly expressed in the venom proteomes. In contrast, such contamination is not expected to affect our results for RGs and ILGs which are harvested prior to dissection of VGs, and the proteins found in these glands were also indicated in their transcriptomes with reasonable qualitative and quantitative agreement between proteomes and transcriptomes.

In summary, the very low expression level of toxins and the trace quantities detected in HGs rule out a contribution of this gland to the venom cocktail. This agrees with a recent report that characterized the transcriptome of the HGs of three colubroid snakes and detected a low level of expression of toxins (Dominguéz-Pérez et al., 2019). These authors suggested that the low expression of toxins indicates that their biological roles is related to protection against harmful microorganisms and viruses, infections in the orbital space, mucosal membranes, and skin, rather than predation.

In micrurine snakes, lipocalin was highly expressed in all species studied (Table 1, Table S4 in Supplementary file 2). Other nontoxin transcripts that are highly expressed in HGs are sperm protamine, lipocalin/fatty-acid binding family protein, and bactericidal/permeability-increasing-like protein (BPI) fold-containing family B member (Table 1, Table S4 in Supplementary file 2). We also detected coding sequences without homologous sequences in any searched databases (uncharacterized proteins) with unknown functions (Table S4 in Supplementary file 2).

Recent reports of expression profiles of HGs in snakes are in accordance with our results for the New World coral snakes, specifically the predominance of the lipocalin protein family in proteomic data for the HG of *Thamnophis sirtalis* (Steglich et al., 2019), and high expression of transcripts of transport/binding, lipocalin/lipocalin-like, and bactericidal/permeability-increasing-like proteins were highly expressed in HGs (Domínguez-Pérez et al., 2019). Additionally, these authors suggested that HG-specific lipocalin may function as a transport protein associated with VNO olfaction. This lipocalin contains a signal peptide, as expected for a secreted protein, and it is highly expressed in HGs but not in other tissues, including the secretory tissue, and Duvernoy's (venom) gland (Steglich et al., 2019). Lipocalins constitute a family of small extracellular proteins of great functional diversity, with roles in the transport of proteins and pheromones, olfaction, regulation of cell homeostasis and the modulation of the immune response (Flower, 1996). Lipocalins have been found in transcriptomes or by RT-PCR amplification of several snake glands (Fry et al., 2012). In the VG of *Atractaspis aterrima*, some sequences of lipocalins were identified among the highly expressed transcripts (Terrat et al., 2013). Lipocalins were also found in *Oxyrhopus guibei* (Junqueira-de-Azevedo et al., 2016). These identified lipocalins were putatively associated with allergen (Fry et al., 2012), but the functional roles of lipocalins in snakes are still unknown. In micrurine snakes, lipocalins are highly expressed in HGs and not expressed in the other glands investigated suggesting that this protein family is an important in HG function, which may involve several biological processes, including nasal and/or VNO olfaction. We recognized a high number of lipocalins in the proteomes of the HGs (Table S4 in Supplementary file 2). In the four species of *Micrurus* investigated, the sequences of lipocalin sequences showed high similarity with the previously identified lipocalin of *Naja naja* and *Oxyrhopus guibei*.

Additionally, we found that bactericidal/permeability-increasing-like protein is highly expressed in the HGs (Table S4 in Supplementary file 2). The presence of bactericidal proteins in this gland indicates potential involvement in the previously suggested (Domínguez-Pérez et al., 2019) defence against pathogens and immune response. The family of the bactericidal/permeability-increasing-like proteins is associated with protection against Gram-negative bacteria in vertebrates, besides other functions such as odorant carrier or removal (Andrault et al., 2003; Zhou et al., 2014; Olender et al., 2016). This result agrees with recent findings that observed a significant amount of bactericidal/permeability-increasing-like protein in the HG transcriptomes of some colubroid snakes and with the enrichment analysis of the HG in *Thamnophis sirtalis parietalis* (Domínguez-Pérez et al., 2019; Bentz, 2019). As the HG secretion is transported to the VNO via the nasolacrimal duct, it is expected that its antimicrobial proteins are associated with the protection of the VNO epithelium, which is often in contact with environmental pathogens (Bentz, 2019).

The presence of transcripts with no significant similarity or uncharacterized proteins in the HGs of *Micrurus* indicates that a significant part of the secretion of this gland remains unknown. Similar results were found in studies that characterized HG proteins in other snake species (Steglich et al., 2019; Bentz, 2019). Among the most expressed transcripts of HG from *Micrurus*, we identified sequences classified as sperm protamine P1-like (Table S4 in Supplementary file 2). However, although these transcripts were found in all four species investigated, the low similarity with sperm protamine sequences from the other snakes (<70% of query coverage and <80% of the identity; Table S4 in Supplementary file 2) prevents us from determining whether these sequences in fact belong to the protamine family. Furthermore, the function of the protamine is related to the compaction of sperm DNA into a highly condensed complex during the spermatogenesis (Balhorn, 2007), which has no clear relationship to the putative functions of HGs.

3.4. Comparing the expression profiles of glands and predicting their biological function

For comparative transcriptomic analysis, we inferred orthologous transcripts across the four species studied. We identified 4395 orthogroups representing *bona fide* orthologous relationships and used their expression data to perform a principal component analysis (PCA). As expected, the PCA revealed that the gene expression allows clustering of homologous tissues rather than species (Sudmant et al., 2015; Barua and Mikheyev, 2021) and differences among glands explain more than 50% of the variation present in the data (Fig. 5A). HG samples cluster tightly and distant from other oral glands reflecting that HGs have a neat and distinct expression profile and indicating distinctive. VG samples clustered tightly, distant from the HG cluster and slightly closer the ILG and RG clusters. The distinct placement of the VG cluster may be related to its expression profile directed to the active production of toxin genes. However, RG and ILG cluster together indicating similar expression profiles and high homology: ILG and RG tissues share a common set of genes expressed at a similar level (Fig. 5B, Table 1), quite different from VGs and HGs.

To ensure that the patterns observed for the VG, ILG and RG clusters were not biased by the toxin gene expression, we also performed an analysis after removing the toxin orthogroups (Fig. S3 in Supplementary file 3). This analysis revealed that the variance in the main component (PC1) was maintained and only differences in the second component changed (PC2) consistent with VGs presenting a distinct expression pattern that may be related to the specialized functions of high toxin production. Decrease in the PC2 distance when removing the toxin orthogroups suggests that VG, ILG and RG share a similar active network of expressed genes. It has been previously shown that oral and salivary

glands may present a gene expression profile like that presented by VGs, which may allow any of these oral glands to produce toxins (Barua and Mikheyev, 2021). In this sense, the low level of toxins observed in the non-VGs (Figs. 4 and 5B, and Table 1) may represent the basal expression in which the evolutionary processes may act to select higher toxin expression levels and turn an ordinary oral gland into a venom factory. Venom variation may be associated with sub-modules of expression within toxins and their regulatory genes, and this modular expression may be a key mechanism to venom evolution (Mason et al., 2020; Barua and Mikheyev, 2021; Nachtigall et al., 2022). Thus, the set of genes shared between the VG and the oral glands investigated (i.e., ILG and RG) may represent modules related to the metavenom network that may be responsible for toxin production in these glands (Barua and Mikheyev, 2021), and which is highly active in the VGs and much less in ILGs and RGs. Further epigenetics experiments using these glands will be needed to better understand the specific regulatory networks and support such hypothesis.

Based on the differing expression data observed among glands, we predicted the biological processes involving each gland using Gene Ontology (GO) enrichment (Fig. 6). For VGs, we detected enriched GO terms associated with the pronounced secretory function of VGs during venom production (Perry et al., 2020). These terms were associated with the processes of translation, protein transport, and protein modification. However, we also identified that processes related to the regulation of enzyme activity were highly active, which may be a response to inhibit the toxic activity of venom during production and storage. These biological processes detected may be an auxiliary source of self-protection of the VG by complementing the acidification processes observed in the lumen of the VG (Mackessy and Baxter, 2006).

ILG and RG expression profiles are very similar, and the GO enrichment analysis revealed that these glands may be involved in protein production, inhibition and activation of peptidase activity, and immune response to external pathogens. The enrichment analysis performed here identified gene sets that were enriched in both ILG and RG and were related to the defence response, such as response to other organisms, responses to bacterium, and immune responses (Fig. 6). This indicates that both glands may be acting as the first barrier of the immune system by highly expressing immunoglobulins, to recognize and bind to antigens, and chitotriosidase, to active macrophage activity and promotes defence-associated functions (Fig. 5B, Table 1, and Table S9 in Supplementary file 1). In addition to immunoglobulin and chitotriosidase, the highly expressed ficolins in ILGs and RGs have been associated with the innate immune response in mammals (Bidula et al., 2019), and may also have some type of function in this regard in snakes.

For HGs, we noticed highly active metabolic processes and protein transport, which may be related to the high production and export of several biochemicals acting on several biological activities, including olfactory and/or VNO senses. These results agree with the enrichment analysis of the HG in *Thamnophis sirtalis parietalis*, where a high number of GO terms were related to the production and transport of proteins to the Golgi and to the production and transport of glycoproteins (Bentz, 2019). Moreover, the HG produces a high amount of lipocalin that may be an important transporter of biomolecules, such as pheromones, steroids, bilins, retinoids, lipids, and polymers (Flower, 1996; Glasgow, 2021). The high expression of lipocalin and lipocalin/fatty-acid binding protein in the HG (Fig. 5B, Table 1, and Table S4 in Supplementary file 2) suggests that it may be associated with several binding and or transport molecules with diverse biological functions. For example, a significant enrichment of genes associated with the GO term for lipid-binding in the HG of the snake *Thamnophis sirtalis parietalis* was associated with the transport of attractive pheromones in this species (Bentz, 2019). Given that the pheromone is non-polar and insoluble in aqueous media, Bentz (2019) suggests it must be bound to a protein to become soluble and transported into the VNO lumen. In summary, several biological roles may be associated with this gland, such as the transport of pheromones and/or odorants to the VNO, immune response and antimicrobial activity, and retinoid binding.

The present study allowed us to infer biological processes for each gland; however, the processes and functions inferred may be limited by the divergence time of the reference and the target species. Specifically, we used the chicken as reference, which is a distantly related species, to infer the biological processes within each gland. Despite the estimated 230 millions of years of divergence time between snakes and birds (Kumar et al., 2017), the chicken genome represented a related species containing the most complete set of genes with associated functional roles. Unfortunately, any other closely related species, such as any snake or lizard species, presents a complete set of genes with a reliable functional characterization. The limitation of using a distantly related species can be related to differences in biological processes active in the glands and genes of the reference (i.e., chicken) and the target species (i.e., coral snakes). For instance, our analysis may be hiding some active processes in each gland because these biological processes are not assigned to the chicken orthologous genes. Our analysis may also be inferring biological roles not active in the snake's glands because the orthologous genes in snakes may have evolved to act in distinct pathways than that associated to the chicken genes. In this sense, our analysis allowed us to predict the active biological processes in each gland, but it may represent an incomplete scenario. Of note, it is a limitation faced by any research focusing on better understanding the biology of understudied organisms (a.k.a., non-model species). Further experimental studies must be designed to better understand the biological roles of the analysed glands in coral snakes to confirm the inferences and hypothesis of the present study.

4. Conclusions

VGs of the New World coral snakes are conserved in terms of morphology in relation to other elapids. *Micruroides* differs from other New World elapids in lacking the posterior inflection of the VG. In snakes of the genus *Micrurus*, the VG has high toxin expression in all species investigated. The VG is a venom production gland, and its machinery is invested in protein production, maturation, and export. Two distinct glands (ILG and the inferior RG) are recognized in the mandibular area of all studied species. The inferior RG is well-developed in all species of the genus *Micrurus*, but it is small in *Micruroides*, while the presence of the superior RG gland is highly variable. Despite their distinct morphologies, the ILGs and inferior RGs of *Micrurus* present similar expression profiles, and the biological process prediction showed that they may act in the protein production, inhibition and activation of peptidase activity, and immune response to external pathogens. RGs and ILGs produce toxin types that are frequently found in VGs. CTL and CRISP are more expressed in these glands than in VG, suggesting additional function for these glands. However, the low levels of expression of the key toxin types (3FTx, PLA_2 and Kunitz) in these glands compared to VG, may also indicate a basal gene expression expected to occur in any oral/salivary glands due to the common set of genes within the metavenom network active in these tissues. Although restricted to the orbit, the HGs of micrurines is well-developed and occupies most of the area between the lateral surface of the frontal bone and medial surface of the eye. HGs are highly divergent from the other glands and its expression profiles indicates that it is an important organ related to the production of biomolecules that may function in several pathways, such as protection of VNO epithelium, transport of pheromones, and transport of biochemicals related to the VNO sensing. As there is no connection between the duct of the HG and ocular structures in the micrurines, functions associated with eye physiology and protection through "tears" are not likely for the HG secretions of these snakes. Expanding the set of glands and species investigated and integrating the expression data with epigenetic experiments may help to better decipher the functional roles of these glands in the snake's biology.

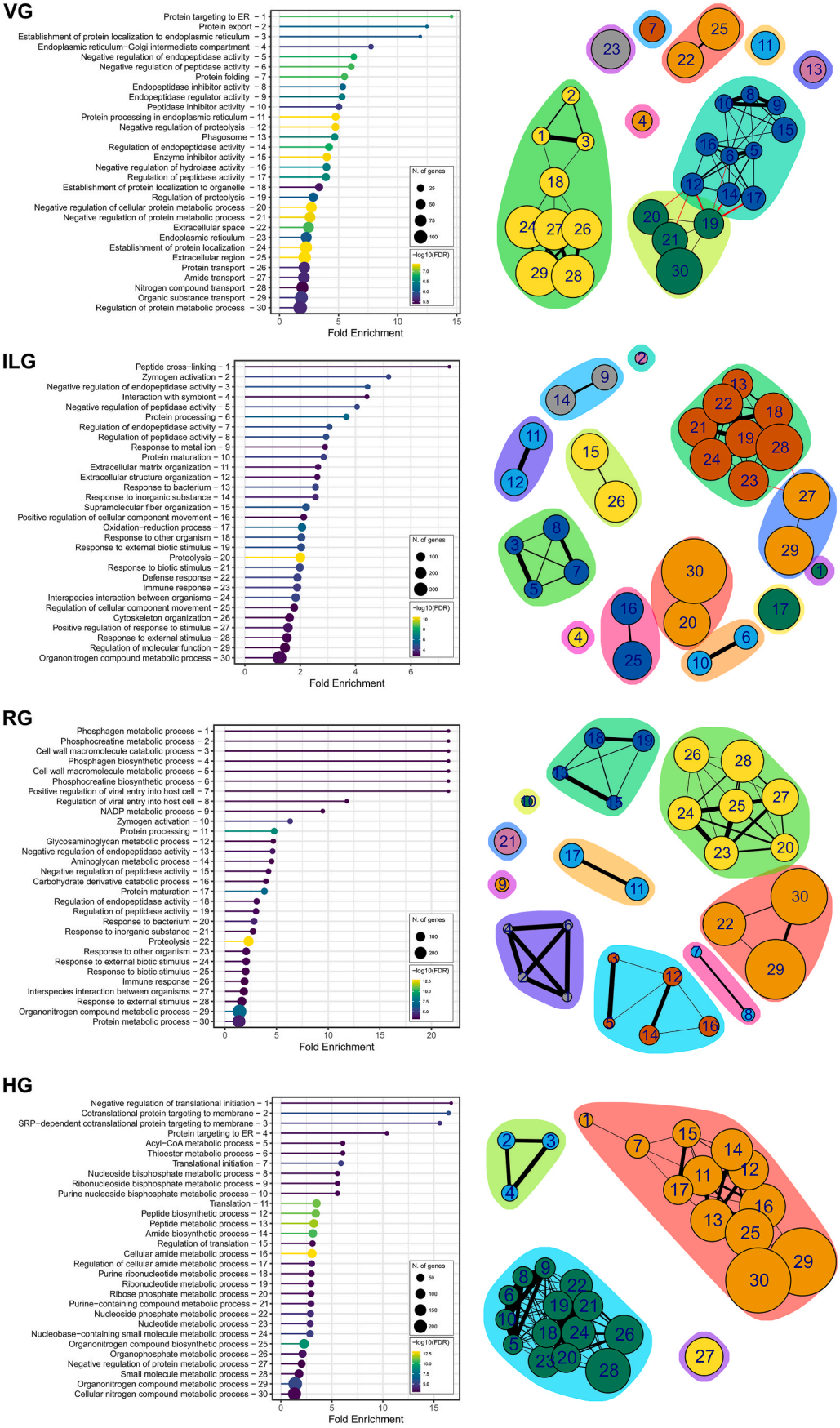

Fig. 6. Functional characterization of gene expression in the cephalic glands (VG, ILG, RG, and HG) of *Micrurus* species. Left: List of enriched GO terms detected in each gland studied. Right: Network of all significantly enriched GO terms (i.e., nodes of the network) and genes shared among them (i.e., edges of the network) detected in each gland. The GO terms are numbered following the left chart. Two nodes are connected if they share greater than 20% of their genes. Node size corresponds to size of the gene sets and edge thickness corresponds to the number of overlapped genes. The coloured envelopes represent modules with dense nodal connections, but sparse connections to other modules.

Credit author statement

LO, PGN, VLV, MW and ILMJA conceived and designed the experiments. LO performed the morphological experiments. LO, PGN, PFC, and VLV performed the RNA-seq and proteome experiments. PGN performed the bioinformatics analysis. ACN and LO performed the immunohistochemical experiments. LO and PGN wrote the manuscript. All authors read, critically edited, and approved the final manuscript.

Funding

This research was supported by grants from Fundação de Amparo à Pesquisa do Estado de São Paulo (FAPESP) to LO (FAPESP 2017/25089-5 and 2018/09301-7), PGN (FAPESP 2018/26520-4), and ILMJA (BIOTA/FAPESP 2016/50127-5). ILMJA and HZ are supported by Conselho Nacional de Desenvolvimento Científico e Tecnológico - CNPq. NJS is a Scientific Productivity Scholarship holder (Level 2) from the Brazilian National Council of Technological and Scientific Development (CNPq) (314287/2020-5).

Ethical statement

All experimental procedures were reviewed and approved by the Ethics Committee on Animal Use of the Instituto Butantan (CEUAIB; Protocol Number 4479020217). The specimens used in the present study were registered in the Brazilian National System for the Management of Genetic Heritage and Associated Traditional Knowledge (SisGen; Registration Number A6E9C41). The species were collected under the permits from Instituto Chico Mendes de Conservação da Biodiversidade (ICMBio; permit numbers 56576, 57585 and 66597). The authors compiled with the ARRIVE guidelines (https://arriveguidelines.org/arrive-guidelines).

Declaration of competing interest

The authors declare that they have no known competing financial interests or personal relationships that could have appeared to influence the work reported in this paper.

Data availability

Data will be made available on request.

Acknowledgments

We thank Patrick Campbell (NHM, UK) and Valdir J. Germano (Instituto Butantan, Brazil) for allowing and facilitating the study and preparation of specimens under their care and Alberto B. Carvalho and Rosely Rodrigues da Silva (Laboratory of Microtomography of the Museum of Zoology, University of São Paulo, Brazil), and Vincent Fernandez and Brett Clark (Laboratory of Computed Tomography, Imaging and Analysis Centre, NHM, UK) for helping in acquiring and processing tomography images. We also thank Gesiele Almeida Barros de Carvalho (Instituto Butantan, Brazil) for additional help with bioinformatics approaches and Paula Carolina Rodrigues de Almeida (Museu Paraense Emílio Goeldi, Brazil) for help with specimens at the beginning of this work.

Appendix A. Supplementary data

Supplementary data to this article can be found online at https://doi.org/10.1016/j.toxicon.2023.107285.

References

Ahmed, M., Rocha, J.B.T., Morsh, V.M., Schetinger, R.C., 2010. Snake venom acetylcholinesterase. In: Mackessy, S.P. (Ed.), Handbook of Venoms and Toxins of Reptiles. CRC Press Taylor & Francis Group, 207–2019.

Aird, S.D., Watanabe, Y., Villar-Briones, A., Roy, M.C., Terada, K., Mikheyev, A., 2013. Quantitative high-throughput profiling of snake venom gland transcriptomes and proteomes (*Ovophis okinavensis* and *Protobothrops flavoviridis*). BMC Genom. 14, 790. https://doi.org/10.1186/1471-2164-14-790.

Aird, S.D., Da Silva Jr., N.J., Qiu, L., Villar-Briones, A., Saddi, V.A., Telles, M.P.C., Grau, M.L., Mikheyev, A.S., 2017. Coralsnake venomics: analyses of venom gland transcriptomes and proteomes of six Brazilian taxa. Toxins 9, 187. https://doi:10.3390/toxins9060187.

Amorin, F.G., Costa, T.F., Baiwir, D., Pauw, E.D., Quinton, L., Sampaio, S.V., 2018. Proteopeptidomic, function and immunoreactivity characterization of *Bothrops moojeni* snake venom: influence of snake gender on venom composition. Toxins 10, 177. https://doi:10.3390/toxins10050177.

Andrault, J.B., Gaillard, I., Giorgi, D., Rouquier, S., 2003. Expansion of the bpi family by duplication on human chromosome 20: characterization of the RY gene cluster in 20q11. 21 encoding olfactory transporters/antimicrobial-like peptides. Genomics 82, 172–184. https://doi:10.1016/s0888-7543(03)00102-2.

Ashburner, M., Ball, C.A., Blake, J.A., Botstein, D., Butler, H., Cherry, J.M., Davis, A.P., Dolinski, K., Dwight, S.S., Eppig, J.T., Harris, M.A., Hill, D.P., Issel-Tarver, L., Kasarskis, A., Lewis, S., Matese, J.C., Richardson, J.E., Ringwald, M., Rubin, G.M., Sherlock, G., 2000. Gene ontology: tool for the unification of biology. The Gene Ontology Consortium. Nat. Genet. 25 (1), 25–29. https://doi:10.1038/75556.

Balhorn, R., 2007. The protamine family of sperm nuclear proteins. Genome Biol. 8, 227. https://doi.org/10.1186/gb-2007-8-9-227.

Barua, A., Mikheyev, A.S., 2021. An ancient, conserved gene regulatory network led to the rise of oral venom systems. Proc. Natl. Acad. Sci. USA 118, 14. https://doi.org/10.1073/pnas.2021311118.

Bellairs, A.D.'A., Boyd, J.D., 1947. The lachrymal apparatus in lizards and snakes. – I. The brille, the orbital glands, lachrymal canaliculi and origin of the lachrymal duct. Proc. Zool. Soc. Lond. 117, 81–108. https://doi.org/10.1111/j.1096-3642.1947.tb00500.x.

Bellairs, A.D.'A., Boyd, J.D., 1949. The lachrymal apparatus in lizards and snakes. – II. The Anterior part of the lachrymal duct and its relationship with the palate and with the nasal and vomeronasal organs. Proc. Zool. Soc. Lond. 120, 269–310. https://doi.org/10.1111/j.1096-3642.1950.tb00949.x.

Bentz, E.J., 2019. Characterizing the Function of the Harderian Gland and its Interaction with the Vomeronasal Organ in the Red-Sided Garter Snake, *Thamnophis sirtalis Parietalis*. Unpublished Doctor of Philosophy thesis. Oregon State University.

Bidula, S., Sexton, D.W., Schelenz, S., 2019. Ficolins and the recognition of pathogenic microorganisms: an overview of the innate immune response and contribution of single nucleotide polymorphisms. J. Immune Res. 2019, 3205072 https://doi.org/10.1155/2019/3205072.

Braga, J.R.M., Morais-Zani, K., Pereira, D.S., Sant'Anna, S.S., Galizio, N.C., Tanaka-Azevedo, A.M., Vilarinho, A.R.G., Rodrigues, J.L., Rocha, M.M.T., 2020. Sexual and ontogenetic variation of *Bothrops leucurus* venom. Toxicon 184, 127–135. https://doi.org/10.1016/j.toxicon.2020.05.028.

Brown, R.M., Smart, U., Levrron, A.E., Smith, E.N., 2018. A new species of long-glanded coralsnakes of the genus *Calliophis* (Squamata: Elapidae) from Dinagat island, with notes on the biogeography and species diversity of Philippine *Calliophis* and *Hemibungarus*. Herpetologica 74, 89–104. https://doi.org/10.1655/Herpetologica-D-17-00008.

Bucaretchi, F., Capitani, M.E., Hyslop, S., 2021. Chapter 21 – coralsnake envenomations in Brazil. In: da Silva Jr, N.J., Porras, L.W., Aird, S.D., Prudente, A.L.C. (Eds.), Advances in Coralsnake Biology: with an Emphasis on South America. Eagle Mountain Publishing, LC, Eagle Mountain, Utah, pp. 703–744.

Burns, B., Pickwell, G.V., 1972. Cephalic glands in sea snakes (*pelamis, hydrophis* and *Laticauda*). Copeia 1972, 547–559. https://doi.org/10.2307/1442929.

Bushmanova, E., Antipov, D., Lapidus, A., Prjibelski, A.D., 2019. rnaSPAdes: a de novo transcriptome assembler and its application to RNA-Seq data. GigaScience 8 (9). https://doi.org/10.1093/gigascience/giz100 giz100.

Campbell, J.A., Lamar, W.W., 1989. The Venomous Reptiles of Latin America. Comstock Publishing Associates. Cornell University Press, Ithaca. New York.

Campbell, J.A., Lamar, W.W., 2004. The Venomous Reptiles of Western Hemisphere, ume I. Comstock Publishing Associates. Cornell University Press, Ithaca. New York.

Chang, Z., Li, G., Liu, J., Zhang, Y., Ashby, C., Liu, D., Cramer, C.L., Huang, X., 2015. Bridger: a new framework for de novo transcriptome assembly using RNA-seq data. Genome Biol. 16, 1–10. https://doi.org/10.1186/s13059-015-0596-2.

Corrêa-Netto, C., Junqueira-de-Azevedo, I.L.M., Silva, D.A., Ho, P.L., Leitão-de-Araujo, M., Alves, M.L.M., Sanz, L., Foguel, D., Zingali, R.B., Calvete, J.J., 2011. Snake venomics and venom gland transcriptomic analysis of Brazilian coral snakes, *Micrurus altirostris* and *M. corallinus*. J. Proteonomics 74, 1795–1809. https://doi.org/10.1016/j.jprot.2011.04.003.

Csárdi, G., Nepusz, T., 2006. The igraph software package for complex network research. Int. J. Complex Syst. 1659, 1–9.

Dashevsky, D., Fry, B.G., 2018. Ancient diversification of three-finger toxins in *Micrurus* coral snakes. J. Mol. Evol. 86, 58–67. https://doi.org/10.1007/s00239-017-9825-5.

Dashevsky, D., Rokyta, D., Frank, N., Nouwens, A., Fry, B.G., 2021. Electric blue: molecular evolution of three-finger toxins in long-glanded coral snake species *Calliophis bivirgatus*. Toxins, 2021 13, 124. https://doi.org/10.3390/toxins13020124.

Dix, M.W., 1978. A venom gland in the lower jaw of the coral snake (*Micrurus nigrocintus mosquitensis* Schmidt). In: Rosenberg, P. (Ed.), Toxin, Animal, Plant and Microbial. Pergamon Press (Toxicon, Oxford, pp. 16–28. Suppl. Nº 1).

Domínguez-Pérez, D., Duban, J., Agüero-Chapin, G., López, J.T., Molina-Ruiz, R., Almeida, D., Calvete, J.J., Vasconcelos, V., Antunes, A., 2019. The Harderian gland transcriptomes of *Caraiba andreae, Cubophis cantherigerus* and *Tretanorhinus variabilis*, three colubroid snakes from Cuba. Genomics 111, 1720–1727. https://doi.org/10.1016/j.ygeno.2018.11.026.

Emms, D.M., Kelly, S., 2019. OrthoFinder: phylogenetic orthology inference for comparative genomics. Genome Biol. 20, 1–14. https://doi.org/10.1186/s13059-019-1832-y.

Flower, D.R., 1996. The lipocalin protein family: structure and function. Biochem. J. 318, 1–14. https://doi.org/10.1042/bj3180001.

Freitas-de-Sousa, L.A., Nachtigall, P.G., Portes-Junior, J.A., Holding, M.L., Nystrom, G.S., Ellsworth, S.A., Guimarães, N.C., Tioyama, E., Ortiz, F., Silva, B.R., Kunz, T.S., Junqueira-de-Azevedo, I.L.M., Grazziotin, F.G., Rokyta, D.R., Moura-da-Silva, A.M., 2020. Size matters: an evaluation of the molecular basis of ontogenetic modifications in the composition of *Bothrops jararacussu* snake venom. Toxins 12 (12), 791. https://doi.org/10.3390/toxins12120791.

Fry, B.G., 2005. From genome to "venome: molecular origin and evolution of the snake venom proteome inferred from phylogenetic analysis of toxin sequences and related body proteins. Genome Res. 15, 403–420. https://doi.org/10.1101/gr.3228405.

Fry, B.G., Casewell, N.R., Wüster, W., Vidal, N., Young, B., Jackson, T.N.W., 2012. The structure and functional diversification of the Toxicofera reptile venom system. Toxicon 60, 434–448. https://doi.org/10.1016/j.toxicon.2012.02.013.

Fry, B.G., Undheim, E.A.B., Ali, S.A., Jackson, T.N.W., Debono, J., Scheib, H., Ruder, T., Morgenstern, D., Cadwallader, L., Whitehead, D., Nabuurs, R., van der Weerd, L., Vidal, N., Roelants, K., Hendrikx, I., Gonzalez, S.P., Koludarov, I., Jones, A., King, G. F., Antunes, A., Sunagar, K., 2013. Squeezers and leaf-cutters: differential diversification and degeneration of the venom system in toxicoferan reptiles. Mol. Cell. Proteomics 12, 1881–1899. https://doi.org/10.1074/mcp.M112.023143.

Fu, L., Niu, B., Zhu, Z., Wu, S., Li, W., 2012. CD-HIT: accelerated for clustering the next-generation sequencing data. Bioinformatics 28, 3150–3152. https://doi.org/10.1093/bioinformatics/bts565.

Gabe, M., Saint-Girons, H., 1969. Données histologiques sur les glandes salivaires des lépidosauriens. Bull. Mus. Natl. Hist. Nat., n. sér. 58, 1–112.

Gans, C., Kochva, E., 1965. The accessory gland in the venom apparatus of viperid snakes. Toxicon 3, 61–63. https://doi.org/10.1016/0041-0101(65)90069-3.

Ge, S.X., Jung, D., Yao, R., 2019. ShinyGo: a graphical gene-set enrichment tool for animals and plants. Bioinformatics 36, 2628–2629. https://doi.org/10.1093/bioinformatics/btz931.

Giachi, F., Angel, R., Parra, G.J., Delfino, G., 2007. Ultrastructure of the venom gland of the andean red-tailed coral snake *Micrurus mipartitus decussatus* (duméril, bibron & duméril 1854) (squamata serpentes Elapidae). Trop. Zool. 20, 75–89.

Glasgow, B.J., 2021. Tear lipocalin and lipocalin-interacting membrane receptor. Front. Physiol. 12, 684211 https://doi.org/10.3389/fphys.2021.684211.

Gopalakrishnakone, P., 1986. Structure of the venom gland of the Malayan banded snake *Maticora intestinalis*. Snake 18, 19–26.

Gopalakrishnakone, P., Kochva, E., 1990. Venom glands and some associated muscles in sea snakes. J. Morphol. 205, 85–96. https://doi.org/10.1002/jmor.1052050109.

Gopalakrishnakone, P., Kochva, E., 1993. Histological features of the venom apparatus of sea snake *Lapemis curtus*. Snake 25, 27–37.

Haas, B.J., Papanicolaou, A., Yassour, M., Grabherr, M., Blood, P.D., Bowden, J., Couger, M.B., Eccles, D., Li, B., Lieber, M., MacManes, M.D., Ott, M., Orvis, J., Pochet, N., Strozzi, F., Weeks, N., Westerman, R., William, T., Dewey, C., Henschel, R., LeDuc, R.D., Friedman, N., Regev, A., 2013. De novo transcript sequence reconstruction from RNA-seq using the Trinity platform for reference generation and analysis. Nat. Protoc. 8, 1494–1512. https://doi.org/10.1038/nprot.2013.084.

Halstead, B.W., Engen, P.C., Tu, A.T., 1978. The venom and venom apparatus of the sea snake Lapemis hardwicki Gray. Zool. J. Linn. Soc. 63, 371–396. https://doi.org/10.1111/j.1096-3642.1978.tb02100.x.

Hamid, R., Khan, M.A., Ahmad, M., Ahmad, M.M., Abdin, M.Z., Musarrat, J., Javed, S., 2013. Chitinases: an update. J. Pharm. BioAllied Sci. 5, 21–29. https://doi.org/10.4103/0975-7406.106559.

Hillenius, W.J., Rehorek, S.J., 2005. From the eye to the nose: ancient orbital to vomeronasal communication in tetrapods? In: Mason, R., LeMaster, M., MüllerSchwartze, D. (Eds.), Chemical Signals in Vertebrates (10). Kluwer Academic, New York, pp. 228–241.

Hofmann, E.P., Rautsaw, R.M., Strickland, J.L., Holding, M.L., Hogan, M.P., Mason, A.J., Rokyta, D.R., Parkinson, C.L., 2018. Comparative venom-gland transcriptomics and venom proteomics of four Sidewinder Rattlesnake (*Crotalus cerastes*) lineages reveal little differential expression despite individual variation. Sci. Rep. 8, 1–15, 0.1038/s41598-018-33943-5.

Holding, M.L., Margres, M.J., Mason, A.J., Parkinson, C.L., Rokyta, D.R., 2018. Evaluating the performance of de novo assembly methods for venom-gland transcriptomics. Toxins 10, 249. https://doi.org/10.3390/toxins10060249.

Jackson, T.N.W., Young, B., Underwood, G., McCarthy, C.J., Kochva, E., Vidal, N., Weerd, L. van der, Nabuurs, R., Dobson, J., Whitehead, D., Vonk, F.J., Hendrikx, C. H., Fry, B.G., 2017. Endless forms most beautiful: the evolution of ophidian oral glands, including the venom system, and the use of appropriate terminology for homologous structures. Zoomorphology 136, 107–130. https://doi.org/10.1007/s00435-016-0332-9.

Jiang, Y., Li, Y., Lee, W., Xu, X., Zhang, Y., Zhao, R., Zhang, Y., Wang, W., 2011. Venom gland transcriptomes of two elapid snakes (*Bungarus multicinctus* and *Naja atra*) and evolution of toxin genes. BMC Genom. 12, 1. https://doi.org/10.1186/1471-2164-12-1.

Junqueira-de-Azevedo, I.L.M., Campos, P.F., Ching, A.T.C., Mackessy, S.P., 2016. Colubrid venom composition: an -Omics perspective. Toxins 8, 230. https://doi.org/10.3390/toxins8080230.

Kanneganti, M., Kamba, A., Mizoguchi, E., 2013. Role of chitotriosidase (chitinase 1) under normal and disease conditions. J. Epithelial Biol. Pharmacol. 5, 1–9. https://doi.org/10.2174/1875044301205010001.

Kardong, K.V., 2002. Colubrid snakes and Duvernoy's "Venom" glands. J. Toxicol. Toxin Rev. 21, 1–19. https://doi.org/10.1081/TXR-120004739.

Kochva, E., 1978. Oral glands of the reptilia. In: Gans, C., Gans, K.A. (Eds.), Biology of the Reptilia, Physiology B. Academic Press, London, pp. 43–161.

Kochva, E., 1987. The origin of snakes and evolution of the venom apparatus. Toxicon 25, 65–106. https://doi.org/10.1016/0041-0101(87)90150-4.

Koludarov, I., Jackson, T.N.W., Brouw, B.O.d., Dobson, J., Dashevsky, D., Arbuckle, K., Clemente, C.J., Stockdale, E.J., Cochran, C., Debono, J., Stephens, C., Panagides, N., Li, B., Manchadi, M.L.R., Violette, A., Fourmy, R., Hendrikx, I., Nouwens, A., Clements, J., Martelli, P., Kwok, H.F., Fry, B.G., 2017. Enter the dragon: the dynamic and multifunctional evolution of Anguimorpha lizard venoms. Toxins 9, 242. https://doi.org/10.3390/toxins9080242.

Kumar, S., Stecher, G., Suleski, M., Hedges, S.B., 2017. TimeTree: a resource for timelines, timetrees, and divergence times. Mol. Biol. Evol. 34 (7), 1812–1819. https://doi.org/10.1093/molbev/msx116.

Langmead, B., Salzberg, S.L., 2012. Fast gapped-read alignment with Bowtie 2. Nat. Methods 9, 357. https://doi.org/10.1038/nmeth.1923.

Leão, L.I., Ho, P.L., Junqueira-de-Azevedo, I.L.M., 2009. Transcriptomic basis for an antiserum against *Micrurus corallinus* (coral snake) venom. BMC Genom. 10, 112. https://doi.org/10.1186/1471-2164-10-112.

Li, B., Dewey, C.N., 2011. RSEM: accurate transcript quantification from RNA-Seq data with or without a reference genome. BMC Bioinf. 12, 323. https://doi.org/10.1186/1471-2105-12-323.

Lomonte, B., Rey-Suárez, P., Fernández, J., Sasa, M., Pla, D., Vargas, N., Bénard-Valle, M., Sanz, L., Corrêa-Netto, C., Núñez, V., Alape-Girón, A., Alagón, A., Gutiérrez, J.M., Calvete, J.J., 2016. Venoms of *Micrurus* coral snakes: evolutionary trends in compositional patterns emerging from proteomic analyses. Toxicon 122, 7–25. https://doi.org/10.1186/1471-2105-12-323.

Love, M., Huber, W., Anders, S., 2014. Moderated estimation of fold change and dispersion for RNA-seq data with DESeq2. Genome Biol. 15, 550. https://doi.org/10.1186/s13059-014-0550-8.

Mackessy, S.P., Baxter, L.M., 2006. Bioweapons synthesis and storage: the venom gland of front-fanged snakes. Zool. Anz. 245, 147–159. https://doi.org/10.1016/j.jcz.2006.01.003.

Margres, M.J., Aronow, K., Loyacano, J., Rokyta, D.R., 2013. The venom-gland transcriptome of the eastern coral snake (*Micrurus fulvius*) reveals high venom complexity in the intragenomic evolution of venoms. BMC Genom. 14 (1), 1–18. https://doi.org/10.1186/1471-2164-14-531.

Marques, O.A.V., Sazima, I., 2021. Chapter 7: the natural history of New World coralsnakes. In: da Silva Jr, N.J., Porras, L.W., Aird, S.D., Prudente, A.L.C. (Eds.), Advances in Coralsnake Biology: with an Emphasis on South America. Eagle Mountain Publishing, LC, Eagle Mountain, Utah, pp. 275–289.

Mason, A.J., Margres, M.J., Strickland, J.L., Rokyta, D.R., Sasa, M., Parkinson, C.L., 2020. Trait differentiation and modular toxin expression in palm-pitvipers. BMC Genom. 21, 1–20. https://doi.org/10.1186/s12864-020-6545-9.

McCarthy, C.J., 1985. Morphology of elapid snakes (Serpentes: Elapidae). An assessment of the evidence. Zool. J. Linn. Soc. 83, 79–93. https://doi.org/10.1111/j.1096-3642.1985.tb00873.x.

McDowell, S.B., 1968. Affinities of the snakes usually called *Elaps lacteus* and *E. dorsalis*. Zool. J. Linn. Soc. 47 (313), 561–578. https://doi.org/10.1111/j.1096-3642.1968.tb00550h.x.

McDowell, S.B., 1986. The architecture of the corner of the mouth of Colubroid snakes. J. Herpetol. 20, 353–407. https://doi.org/10.2307/1564502.

Metscher, B.D., 2009. MicroCT for comparative morphology: simple staining methods allow high-contrast 3D imaging of diverse nonmineralized animal tissues. BMC Physiol. 9, 1–14. https://doi.org/10.1186/1472-6793-9-11.

Modahl, C.M., Mrinalini, S.F., Mackessy, S.P., 2018. Adaptive evolution of distinct prey-specific toxin genes in rear-fanged snake venom. Proc. R. Soc. A 285, 20181003. https://doi.org/10.1098/rspb.2018.1003.

Modahl, C.M., Saviola, A.J., Mackessy, S.P., 2021. Integration of transcriptomic and proteomic approaches for snake venom profiling. Expert Rev. Proteomics 18, 827–834. https://doi.org/10.1080/14789450.2021.1995357.

Nachtigall, P.G., Rautsaw, R.M., Ellsworth, S.A., Mason, A.J., Rokyta, D.R., Parkinson, C. L., Junqueira-de-Azevedo, I.L.M., 2021a. ToxCodAn: a new toxin annotator and guide to venom gland transcriptomics. Brief. Bioinform. 22 https://doi.org/10.1093/bib/bbab095 bbab095.

Nachtigall, P.G., Kashiwabara, A.Y., Durham, A.M., 2021b. CodAn: predictive models for precise identification of coding regions in eukaryotic transcripts. Brief. Bioinform. 22 https://doi.org/10.1093/bib/bbaa045 bbaa045.

Nachtigall, P.G., Freitas-de-Sousa, L.A., Mason, A.J., Moura-da-Silva, A.M., Grazziotin, F. G., Junqueira-de-Azevedo, I.L.M., 2022. Differences in PLA_2 constitution distinguish the venom of two endemic Brazilian mountain lanceheads, *Bothrops cotiara* and *Bothrops fonsecai*. Toxins 14, 237. https://doi.org/10.3390/toxins14040237.

Nguyen, L.T., Schmidt, H.A., Von Haeseler, A., Minh, B.Q., 2015. IQ-TREE: a fast and effective stochastic algorithm for estimating maximum-likelihood phylogenies. Mol. Biol. Evol. 32, 268–274. https://doi.org/10.1093/molbev/msu300.

Olender, T., Keydar, I., Pinto, J.M., Tatarskyy, P., Alkelai, A., Chien, M.S., Fishilevich, S., Restrepo, D., Matsunami, H., Gilad, Y., 2016. The human olfactory transcriptome. BMC Genom. 17, 619. https://doi.org/10.1186/s12864-016-2960-3.

Oliveira, L., Zaher, H., 2022. An overview of the morphology of oral glands in snakes. In: Gower, D.J., Zaher, H. (Eds.), The Origin and Early Evolutionary Origin of Snakes. Cambridge University Press, pp. 412–436. https://doi.org/10.1017/9781108938891.

Oliveira, L., Jared, C., Prudente, A.L.C., Zaher, H., Antoniazzi, M.M., 2008. Oral glands in dipsadinae 'goo-eater' snakes: morphology and histochemistry of the infralabial glands in *Atractus reticulatus, Dipsas indica*, and *Sibynomorphus mikanii*. Toxicon 51, 898–913. https://doi.org/10.1016/j.toxicon.2007.12.021.

Oliveira, L., Prudente, A.L.C., Zaher, H., 2014. Unusual labial glands in snakes of the genus *geophis* wagler, 1830 (serpentes: dipsadinae). J. Morphol. 275, 87–99. https://doi.org/10.1002/jmor.20199.

Oliveira, L., Buononato, M.A., Zaher, H., 2021. Chapter 12 – the cephalic glands and venom apparatus of coralsnakes. In: da Silva Jr, N.J., Porras, L.W., Aird, S.D., Prudente, A.L.C. (Eds.), Advances in Coralsnake Biology: with an Emphasis on South America. Eagle Mountain Publishing, LC, Eagle Mountain, Utah, pp. 371–390.

OmPraba, G., Chapeaurouge, A., Doley, R., Devi, K.R., Padmanaban, P., Venkatraman, C., Velmurugan, D., Qingsong, L., Kini, R.M., 2010. Identification of a novel family of snake venom proteins Veficolins from *Cerberus rynchops* using a venom gland transcriptomics and proteomics approach. J. Proteome Res. 9, 1882–1893. https://doi.org/10.1021/pr901044x.

Parson, T.S., 1970. The nose and Jocobsons organ. In: Gans, C. (Ed.), Biology of the Reptilia, vol. 2. Morphology B. Academic Press, London, pp. 99–191.

Perry, B.W., Schield, D.R., Westfall, A.K., Mackessy, S.P., Castoe, T.A., 2020. Physiological demands and signaling associated with snake venom production and storage illustrated by transcriptional analyses of venom glands. Sci. Rep. 20, 18083 https://doi.org/10.1038/s41598-020-75048-y.

Phisalix, M., 1922. Animaux venimeux et venins. 2 vols. Masson & Compagnie, Paris.

Phisalix, M., Caius, R., 1918. L'extension de la fonction venimeuse dans l'ordre entière des ophidiens et son existence chez des familles ou elle n'avait pas été soupçonnée jusqu'içi. J. Physiol. Pathol. Gén. 17, 923–964.

Pla, D., Petras, D., Saviola, A.J., Modahl, C.M., Sanz, L., Pérez, A., Juárez, E., Frietze, S., Dorrestein, P.C., Mackessy, S.P., Calvete, J.J., 2018. Transcriptomics-guided bottom-up and top-down venomics of neonate and adult specimens of the arboreal rear-fanged Brown Treesnakes, *Boiga irregularis*, from Gam. J. Proteomics. 174, 71–84. https://doi.org/10.1016/j.jprot.2017.12.020.

Rehorek, S.J., 1997. Squamate Harderian gland: an overview. Anat. Rec. 248, 301–306. https://doi.org/10.1002/(SICI)1097-0185(199707)248:3<301::AID-AR1>3.0.CO;2-S.

Rehorek, S.J., Hillenius, W.J., Quan, W., Halpern, M., 2000a. Passage of Harderian gland secretions to the vomeronasal organ of *Thamnophis sirtalis* (Serpentes: Colubridae). Can. J. Zool. 78, 1284–1288. https://doi.org/10.1139/z00-047.

Rehorek, S.J., Firth, B.T., Hutchinson, M.N., 2000b. The structure of the nasal chemosensory system in squamate reptiles. 2. Lubricatory capacity of the vomeronasal organ. J. Biosci. 25, 181–190.

Rehorek, S.J., Halpern, M., Firth, B.T., Hutchinson, M.N., 2003. The Harderian gland of two species of snakes: *Pseudonaja textilis* (Elapidae) and *Thamnophis sirtalis* (Colubridae). Can. J. Zool. 81, 357–363. https://doi.org/10.1139/z03-014.

Reyes-Velasco, J., Card, D.C., Andrew, A.L., Shaney, K.J., Adams, R.H., Schield, D.R., Casewell, N.R., Mackessy, S.P., Castoe, T.A., 2015. Expression of venom gene homologs in diverse *Python* tissues suggests a new model for the evolution of snake venom. Mol. Biol. Evol. 32, 173–183. https://doi.org/10.1093/molbev/msu294.

Rincon-Filho, S., Naves-de-Souza, D.L., Lopes-de-Souza, L., Silvano-de-Oliveira, J., Ferreyra, C.B., Costal-Oliveira, F., Guerra-Duarte, C., Chávez-Olórtegui, C., 2020. *Micrurus surinamensis* Peruvian snake venom: cytotoxic activity and purification of a C-type lectin protein (Ms-CTL) highly toxic to cardiomyoblast-derived H9c2 cells. Int. J. Biol. Macromol. 164, 1908–1915. https://doi.org/10.1016/j.ijbiomac.2020.08.033.

Rokyta, D.R., Lemmon, A.R., Margres, M.J., Aronow, K., 2012. The venom-gland transcriptome of the eastern diamondback rattlesnake (*Crotalus adamanteus*). BMC Genom. 13, 312. https://doi.org/10.1186/1471-2164-13-312.

Rokyta, D.R., Margres, M.J., Calvin, K., 2015. Post-transcriptional mechanisms contribute little to phenotypic variation in snake venoms. G3-Genes Genom. Genet. 5, 2375–2382. https://doi.org/10.1534/g3.115.020578.

Rosenberg, H.I., 1967. Histology, histochemistry, and emptying mechanism of the venom glands of some elapid snakes. J. Morphol. 123, 133–156. https://doi.org/10.1002/jmor.1051230204.

Roze, J.A., 1996. Coral Snakes of the Americas: Biology, Identification, and Venoms. Krieger Publishing Company, Malabar. Florida.

Rozewicki, J., Li, S., Amada, K.M., Standley, D.M., Katoh, K., 2019. MAFFT-DASH: integrated protein sequence and structural alignment. Nucleic Acids Res. 47 https://doi.org/10.1093/nar/gkz342. W5–W10.

Saint-Girons, H., 1982. Histologie compareé des glandes orbitaires des Lépidosauriens. Ann. Sci. Nat. Zool. 4, 171–191.

Saint-Girons, H., 1988. Les glandes céphaliques exocrines des Reptiles. I. Données anatomiques et histologiques. Ann. Sci. Nat. Zool. 9, 221–255.

Salomão, M.G., 1991. Estrutura e secreção das glândulas de Duvernoy de Sibynomorphus mikanii (Colubridae, Dipsadinae) e Philodryas olfersii (Colubridae, Xenodontinae), e das glândulas de veneno de Bothrops jararaca (Viperidae, Crotalinae) e Micrurus frontalis (Elapidae, Elapinae) e a influência dos estados de alimentação e jejum. Unpublished Doctor of Philosophy thesis. Instituto de Biociências, University of São Paulo, São Paulo.

Sanz, L., Pla, D., Pérez, A., Rodríguez, Y., Zavaleta, A., Salas, M., Lomonte, B., Calvete, J. J., 2016. Venomic analysis of the poorly studied desert coral snake, *Micrurus tschudii tschudii*, supports the 3FTx/PLA2 dichotomy across *Micrurus* venoms. Toxins 8, 178. https://doi.org/10.3390/toxins8060178.

Sanz, L., Freitas-Lima, L.N., Quesada-Bernat, S., Graça-de-Souza, V.K., Soares, A.M., Calderón, L.A., Calvete, J.J., Caldeira, C.A.S., 2019. Comparative venomics of Brazilian coral snakes: *Micrurus frontalis, Micrurus spixii spixii*, and *Micrurus surinamensis*. Toxicon 166, 39–45. https://doi.org/10.1016/j.toxicon.2019.05.001.

Savitzky, A.H., 1979. The origin of the New World proteroglyphous snakes and its bearing on the study of venom delivery systems in snakes. In: Unpublished Doctor of Philosophy Thesis. University of Kansas, Lawrence.

Schmidt, K.P., 1928. Notes on American coral snakes. Bull. Antiv. Inst. Am. 2, 63–64.

Schmidt, K.P., 1937. The history of *Elaps collaris* SCHLEGEL 1837-1937. Field Mus. Nat. Hist. 20, 361–364.

Silva Jr., Buononato, M.A., Pires, M.G., Feitosa, D.T., 2021a. New World corasnakes: an overview. In: da Silva Jr, N.J., Porras, L.W., Aird, S.D., Prudente, A.L.C. (Eds.), Advances in Coralsnake Biology: with an Emphasis on South America. Eagle Mountain Publishing, LC, Eagle Mountain, Utah, pp. 115–139.

Silva Jr., Feitosa, D.T., Pires, M.G., Prudente, A.L.C., 2021b. Coralsnake diversity in Brazil. In: da Silva Jr, N.J., Porras, L.W., Aird, S.D., Prudente, A.L.C. (Eds.), Advances in Coralsnake Biology: with an Emphasis on South America. Eagle Mountain Publishing, LC, Eagle Mountain, Utah, pp. 141–252.

Slowinski, J.B., 1995. A phylogenetic analysis of the New World coral snakes (Elapidae: *Leptomicrurus, Micruroides*, and *Micrurus*) based on allozymic and morphological characters. J. Herpetol. 29, 325–338. https://doi.org/10.2307/1564981.

Slowinski, J.B., Boundy, J., Lawson, R., 2001. The phylogenetic relationships of Asian coral snakes (Elapidae: *Calliophis* and *Maticora*) based on morphological and molecular characters. Herpetologica 57, 233–245.

Smith, M., Bellairs, A.A., 1947. The head glands of snakes, with remarks on the evolution of the parotid gland and teeth of the opisthoglypha. Zool. J. Linn. Soc. 41, 353–368. https://doi.org/10.1111/j.1096-3642.1940.tb02079.x.

Smith, E.N., Ogale, H., Deepak, V., Giri, V.B., 2012. A new species of coralsnake of the genus *Calliophis* (Squamata: Elapidae) from the west coast of peninsular India. Zootaxa 3437, 51–68. https://doi.org/10.11646/zootaxa.3437.1.5.

Souza, N.M., Maggs, D.J., Park, S.A., Puchalsky, S.M., Reilly, C.M., Paul-Murphy, J., Murphy, C.J., 2015. Gross, histologic, and micro-computed tomographic anatomy of the lacrimal system of snakes. Vet. Ophthalmol. 18, 15–22. https://doi.org/10.1111/vop.12184.

Steglich, S.S., Brown, M.E., Mitchell, E.M., Millen, M., Rehorek, S.J., 2019. Isolation and characterization of abundantly-expressed cDNAs from the harderian gland of the garter snake (*Thamnophis sirtalis*: Colubridae). Comp. Biochem. Physiol., A 234, 22–28. https://doi.org/10.1016/j.cbpa.2019.05.001.

Sudmant, P.H., Alexis, M.S., Burge, C.B., 2015. Meta-analysis of RNA-seq expression data across species, tissues and studies. Genome Biol. 16, 1–11. https://doi.org/10.1186/s13059-015-0853-4.

Taub, A.M., 1966. Ophidian cephalic glands. J. Morphol. 118, 529–542. https://doi.org/10.1002/jmor.1051180406.

Terrat, Y., Sunagar, K., Fry, B.G., Jackson, T.N., Scheib, H., Fourmy, R., Verdenaud, M., Blanchet, G., Antunes, A., Ducancel, F., 2013. *Atractaspis aterrima* toxins: the first insight into the molecular evolution of venom in side-stabbers. Toxins 5, 1948–1964. https://doi.org/10.3390/toxins5111948.

Uetz, P., Freed, P., Aguilar, R., Hošek, J. (Eds.), 2021. The Reptile Database. http://www.reptile-database.org. (Accessed 19 October 2021).

Underwood, G., 1997. An overview of venomous snake evolution. Symposium of Zoological Society of London. In: Thorpe, R.S., Wüster, W., Malhotra, A., snake, Venomous (Eds.), Ecology, Evolution and Snakebite. The Zoological Society of London, vol. 70. Clarendon Press, Oxford, pp. 1–13.

Underwood, G., 2002. On the rictal structures of some snakes. Herpetologica 58, 1–17. https://doi.org/10.1655/0018-0831(2002)058[0001:OTRSOS]2.0.CO;2.

Underwood, G., Kochva, E., 1993. On the affinities of burrowing asps *Atractaspis* (Serpentes: Atractaspididae). Zool. J. Linn. Soc. 107, 3–64. https://doi.org/10.1111/j.1096-3642.1993.tb01252.x.

Valente, R.H., Luna, M.S., de Oliveira, U.C., Nishiyama-Junior, M.Y., Junqueira-de-Azevedo, I.L.M., Portes-Junior, J.A., Clissa, P.B., Viana, L.G., Sanches, L., Moura-da-Silva, A.M., Perales, J., Yamanouye, N., 2018. *Bothrops jararaca* accessory venom gland is an ancillary source of toxins to the snake. J. Proteomics. 177, 137–147. https://doi.org/10.1016/j.jprot.2017.12.009.

Viala, V.L., Hildebrand, D., Trusch, M., Fucase, T.M., Sciani, J.M., Pimenta, D.C., Arni, R. K., Schlüter, H., Betzel, C., Mirtschin, P., Dunstan, N., Spencer, P.J., 2015. Venomics of the Australian eastern brown snake (*Pseudonaja textilis*): detection of new venom proteins and splicing variants. Toxicon 107, 252–265. https://doi.org/10.1016/j.toxicon.2015.06.005.

Vonk, F.J., Casewell, N.R., Henkel, C.V., Heimberg, A.M., Jansen, H.J., McCleary, R.J. R., Kerkkamp, H.M.E., Vos, R.A., Guerreiro, I., Calvete, J.J., Wüster, W., Woods, A. E., Logan, J.M., Harrison, R.A., Castoe, T.A., Koning, A.P.J., Pollock, D.D., Yandell, M., Calderon, D., Renjifo, C., Currier, R.B., Salgado, D., Pla, D., Sanz, L., Hyder, A.S., Ribeiro, J.M.C., Arntzen, J.W., Thillart, G.E.E.J.M., Boetzer, M., Pirovano, W., Dirks, R.P., Spaink, H.P., Doboule, D., McGlinn, E., Kini, R.M., Richardson, M., 2013. The king cobra genome reveals dynamics gene evolution and adaptation in the snake venom system. Proc. Natl. Acad. Sci. USA 110, 20651–20656. https://doi.org/10.1073/pnas.131470211.

Wagler, J., 1824. Serpentum Brasiliensium species novae, ou historie naturelle des espèces nouvelles se serpens. In: de Spix, J. (Ed.), Animalia nova sive species novae. Typis Franc. Seraph, Hübschmanni. Monaco. https://doi.org/10.5962/bhl.title.4269.

Waterhouse, R.M., Seppey, M., Simão, F.A., Manni, M., Ioannidis, P., Klioutchnikov, G., Kriventseva, E.V., Zdobnov, E.M., 2018. BUSCO applications from quality

assessments to gene prediction and phylogenomics. Mol. Biol. Evol. 35, 543–548. https://doi.org/10.1093/molbev/msx319.
Wollberg, M., Kochva, E., Underwood, G., 1998. On the rictal glands of some Atractaspid snakes. Herpetol. J. 8, 137–143.
World Health Organization (WHO), 2010. Guidelines for the Management of Snakebites. New Delhi. India.
Yin, X., Guo, S., Gao, J., Luo, L., Liao, X., Li, M., Su, H., Huang, Z., Xu, J., Pei, J., Chen, S., 2020. Kinetic analysis of effects of temperature and time on the regulation of venom expression in *Bungarus multicinctus*. Sci. Rep. 10, 14142 https://doi.org/10.1038/s41598-020-70565-2.
Young, B.A., Kardong, K.V., 1996. Dentitional surface features in snakes (Reptilia: serpentes). Amphib. -Reptil. 17, 261–276. https://doi.org/10.1163/156853896X00432.
Zaher, H., 1994. Comments on the evolution of the jaw adductor musculature of snakes. Zool. J. Linn. Soc. 111, 339–384. https://doi.org/10.1111/j.1096-3642.1994.tb01488.x.
Zaher, H., 1997. Description of the cephalic muscles and gland morphology of *Clelia plumbea* and three presumably related species (Serpentes, Xenodontinae). Pap. Avuls. Zool. S. Paulo 40, 17–63.
Zaher, H., Oliveira, L.O., Grazziotin, F.G., Campagner, M., Jared, C., Antoniazzi, M.M., Prudente, A.L., 2014. Consuming viscous prey: a novel protein-secreting delivery system in neotropical snail-eating snakes. BMC Evol. Biol. 14, 58. https://doi.org/10.1186/1471-2148-14-58.
Zaher, H., Murphy, R.W., Arredondo, J.C., Graboski, R., Machado-Filho, P.R., Mahlow, K., Montingelli, G.G., Quadros, A.B., Orlov, N.L., Wilkinson, M., Zhang, Y., Grazziotin, F.G., 2019. Large-scale molecular phylogeny, morphology, divergence-time estimation, and the fossil record of advanced caenophidian snakes (Squamata: serpentes). PLoS One 14, e0216148. https://doi.org/10.1371/journal.pone.0216148.
Zaher, H., Grazziotin, F.G., Prudente, A.L.C., Quadros, A.B.A., Trevine, V.C., Silva Jr., N. J., 2021. In: da Silva Jr, N.J., Porras, L.W., Aird, S.D., Prudente, A.L.C. (Eds.), Advances in Coralsnake Biology: with an Emphasis on South America. Eagle Mountain Publishing, LC, Eagle Mountain, Utah, pp. 99–113.
Zhang, J., Kobert, K., Flouri, T., Stamatakis, A., 2014. PEAR: a fast and accurate Illumina Paired-End reAd mergeR. Bioinformatics 30, 614–620. https://doi.org/10.1093/bioinformatics/btt593.
Zhou, Z.P., Xia, X.Y., Guo, Q.S., Xu, C., 2014. Bactericidal/permeability-increasing protein originates in both the testis and the epididymis and localizes in mouse spermatozoa. Asian J. Androl. 16, 309. https://doi.org/10.4103/1008-682X.122583.